

**COMPARISON OF DEFLECTION AND VIBRATION LIMITS FOR HIGH  
PERFORMANCE STEEL BRIDGES**

by

RYAN J. ADAMS

A thesis submitted to the

Graduate School – New Brunswick

Rutgers, The State University of New Jersey

in partial fulfillment of the requirements

for the degree of

Masters of Science

Graduate Program in Civil and Environmental Engineering

written under the direction of

Dr. Hani Nassif

and approved by

---

---

---

New Brunswick, New Jersey

October, 2013

**ABSTRACT OF THE THESIS**  
**COMPARISON OF DEFLECTION AND VIBRATION LIMITS FOR HIGH**  
**PERFORMANCE STEEL BRIDGES**

By RYAN J. ADAMS

Thesis Director:

Dr. Hani Nassif

Deflection limits are used in today's highway bridge industry to indirectly limit the amount of vibration induced under normal operating loads. These limits were established based on subjective human responses to out-dated structure types, and have been found to have no correlation to a bridge's actual vibration behavior or structural longevity. Bridge designers wishing to take advantage of High Performance Steel (HPS) materials are often unnecessarily forced to use heavier girder sections to meet these criteria. This thesis will study the effects of modifying the mass and stiffness of a HPS bridge's main elements to ensure that its vibration levels are within tolerable limits, despite being in violation of the proposed deflection criteria. The analysis will use the grillage method based on a dynamic bridge-road-vehicle interaction system to establish peak accelerations for typical HPS bridges. Parameters such as deck thickness and girder moment of inertia will then be adjusted to bring the structure's vibration to an equivalent level as if the bridge were designed using conventional materials but still meeting deflection limits.

## **ACKNOWLEDGEMENTS**

I would like to thank Dr. Hani Nassif, my thesis advisor, for his guidance and support throughout my graduate career at Rutgers University. Thanks are also given to Dan Su and Ming Liu for their time and helpful input on my research.

I would also like to acknowledge Greenman-Pedersen, Inc for their sponsorship, resources, and encouragement during my Master of Science pursuit.

Lastly, I would like to thank my family and friends, especially my fiancé Hilary, for their patience and support while completing my graduate studies.

## TABLE OF CONTENTS

ABSTRACT OF THE THESIS .....	ii
ACKNOWLEDGEMENTS.....	iii
TABLE OF CONTENTS.....	iv
LIST OF FIGURES .....	vi
LIST OF TABLES.....	viii
CHAPTER 1. INTRODUCTION .....	1
1.1 Problem Statement.....	1
1.2 Scope.....	3
1.3 Organization.....	3
CHAPTER 2. LITERATURE REVIEW .....	5
2.1 Past Research .....	5
2.2 Current Research.....	12
CHAPTER 3. GRILLAGE ANALYSIS METHOD .....	14
3.1 Slab-On-Girder Bridge.....	14
3.2 Bridge Input .....	15
3.2.1 Longitudinal Elements .....	16
3.2.2 Transverse Elements .....	17
3.2.3 System Matrices.....	18
3.2.4 Equivalent Nodal Loads.....	20
3.2.5 Dynamic Equations .....	22
3.3 Road Roughness Input .....	23

3.4 Vehicle Input.....	23
3.5 Output/Computer Processing .....	29
CHAPTER 4. GRILLAGE MODEL DEVELOPMENT.....	32
4.1 Sample Test Bridge.....	32
4.2 Testing Vehicle and Instrumentation Layout.....	36
4.3 Model Assumptions/Idealizations.....	38
4.4 Model Input.....	40
4.5 Calibration Results.....	43
4.6 FEM Calibration .....	47
CHAPTER 5. PARAMETRIC STUDY .....	54
5.1 HPS Bridge Designs .....	54
5.2 Dynamic Modeling .....	58
CHAPTER 6. CONCLUSIONS AND RECOMMENDATIONS .....	65
REFERENCES .....	66

## LIST OF FIGURES

Figure 2.1: Human response to flexibility of girders (Wright and Walker, 1971) .....	8
Figure 2.2: Effect of stringer flexibility of transverse moment in deck (Wright and Walker, 1971) .....	10
Figure 3.1: Typical Slab-on-Girder superstructure .....	15
Figure 3.2: Cross-section properties for grillage members (Liu, 1996) .....	16
Figure 3.3: Wheel load transformation (Liu, 1996) .....	22
Figure 3.4: Vehicle input (Liu, 1996) .....	24
Figure 3.5: Truck mass distribution (Liu, 1996) .....	29
Figure 4.1: Sample structure cross-section (looking north) .....	33
Figure 4.2: Sample structure diaphragm properties .....	34
Figure 4.3: Sample structure framing plan .....	35
Figure 4.4: Test truck .....	36
Figure 4.5: Sensor layout .....	37
Figure 4.6: Grillage element division guideline .....	40
Figure 4.7: Localized area around LVDT 1 showing element division and labels .....	41
Figure 4.8: Localized area around LVDT 1 showing node labels .....	41
Figure 4.9: Lane 1 Southbound deflection results .....	43
Figure 4.10: Lane 2 Southbound deflection results .....	44
Figure 4.11: Spline view of FEM model showing shell and frame elements .....	47
Figure 4.12: Extruded view of FEM model .....	48
Figure 4.13: CSiBridge deck section input form .....	49

Figure 4.14: Barrier section and structural properties .....	50
Figure 4.15: Barrier model assumptions .....	50
Figure 4.16: Test vehicle input .....	52
Figure 4.17: Deflection of LVDT1 node under test vehicle loading .....	53
Figure 5.1: Girder design sections .....	55
Figure 5.2: Graph of HPS design deflection vs. slab thickness .....	57
Figure 5.3: Grade HPS-50W acceleration plots.....	60
Figure 5.4: Grade HPS-70W Hybrid acceleration plots .....	61
Figure 5.5: Grade HPS-100W acceleration plots.....	62
Figure 5.6: Maximum acceleration vs. slab thickness for various HPS bridge designs ....	63

## LIST OF TABLES

Table 1: Historic Depth-to-Span Ratios (ASCE, 1958) .....	6
Table 2: Sample structure girder dimensions .....	33
Table 3: Sample structure test runs .....	38
Table 4: Summary of model calibration results .....	45
Table 5: HPS girder design results using MDX software .....	56
Table 6: Maximum acceleration for HPS bridges.....	59



## CHAPTER 1. INTRODUCTION

### 1.1 Problem Statement

Research and development efforts in the early 1990's led to the introduction of High Performance Steel (HPS), which is available today in yield strengths of 50 ksi, 70 ksi, and 100 ksi. Bridge owners and designers quickly recognized the benefits of this material for its high strength-to-weight ratio, toughness, weldability, and increased corrosion resistance. These properties can produce bridge designs with lighter (shallower) supporting members and fewer splices, generating cost savings for owners with ever-diminishing budgets. However, traditional deflection limits imposed by many bridge owners often prevent designers from taking full advantage of HPS properties resulting in non-uniformity in design outcomes.

Modern deflection criteria is predominantly based on non-rational observations passed down from the railroad bridge industry in the early 20<sup>th</sup> century. Railroad engineers were forced to adhere to stringent deflection limits to prevent rail car wheels from disengaging the tracks under excessive vibration. However, these limits were not rationally derived, as they were established from a collection of empirical case studies. The AASHTO recommended  $\frac{L}{800}$  was originally proposed in the 1930's when the Bureau of Public Roads conducted a survey of a set of sample bridges (the majority constructed of wooden deck planks and superstructure pony trusses or pin-connected through-trusses) that were found to have questionable vibrations based on subjective human responses (ASCE, 1958). The  $\frac{L}{1000}$  limit for pedestrian traffic is even farther from rational beginnings, when

in 1960 a wealthy woman's complaint contending that a bridge's vibration had awoken her sleeping baby as they crossed, sparked immediate action from state engineers to further tighten the allowable limits on bridge deflection (Fountain and Thunman, 1987).

Requiring bridge designers to adhere to outdated criteria that has no rational founding or measurable positive results in terms of increased durability or serviceability severely limits what can be built using today's advances in material and construction technology. Additionally, there is no general consensus on what that criteria should actually be. A survey conducted in 2004 showed that a wide variation exists between U.S. state deflection criteria, with some states requiring  $\frac{L}{1600}$  and others using  $\frac{L}{800}$  (Roeder, et al, 2004). Furthermore, there exists major differences in the state's loading used to compute the deflection. For example:

- One state uses the standard truck alone,
- 16 states use the standard truck plus impact
- 17 states use the standard truck plus lane load plus impact, and
- One state uses lane load only plus impact.

Clearly, current deflection limits offer no consistent benefit for increasing the serviceability of our nation's bridges, and in the case of HPS, can actually penalize owners from fully economizing their structures. Limiting a bridge's deflection has been shown to not control the vibration and acceleration for objectionable human response. There is a need to establish criteria that would help in directly controlling vibration rather than deflection.

## **1.2 Scope**

This thesis will serve as a study to further highlight the disconnect between deflection limits and vibration control for HPS bridges. A traditional composite slab-on-girder bridge will be considered. Based on measured field data, a bridge-road-vehicle model will be calibrated using the grillage method for this sample structure. A 3-D finite-element program will further validate the field data.

Using the grillage model, girder spacing, span length, and roadway width will be held constant for the parametric design of HPS girders of different grades and slab thicknesses. Grades of 50W, 70W, and 100W will be investigated. Attempts will be made to bring HPS designs in violation of deflection limits to vibration levels comparable to designs of lower grades.

## **1.3 Organization**

This thesis will be composed of six chapters. Chapter 1 provides an introduction to the study, scope, and organization of the thesis.

Chapter 2 will present a background of past and current research efforts behind bridge deflection limits.

Chapter 3 will describe the grillage analysis method and program used in this thesis. A brief breakdown of each major input (bridge, roadway, and vehicle) is provided along with the available output data.

Chapter 4 introduces the sample structure, and details the approach used to calibrate the field testing data with the grillage model.

The parametric study is discussed in Chapter 5.

Lastly, Chapter 6 provides conclusions and recommendations.

## **CHAPTER 2. LITERATURE REVIEW**

This chapter presents a comprehensive literature review summarizing past and current studies focusing on superstructure behavior under live-load deflections. The majority of the studies discuss major factors that are influenced by live-load deflection, including structural performance (deck deterioration), bridge vibration, and human response to bridge vibration.

### **2.1 Past Research**

In 1958, the American Society of Civil Engineers (ASCE) Committee on Deflection Limitations of Bridges of the Structural Division (ASCE, 1958) investigated the effect of the deflection limit on deleterious structural effects such as fatigue effects from excessive vibration, excessive stresses due to dynamic loads, and excessive deformation stresses resulting directly from deflection or joint rotation. They also gathered information on human perceptions of bridge vibration, both from pedestrians and vehicle occupants. Whereas the bridge motion itself can be directly attributed to a pedestrian's response, vehicle occupants are also subjected vehicle suspension interactions. The study found no evidence of serious structural damage that could be inferred from excessive live-load deflection or vibration. The committee noted that the original deflection limit was proposed for structures unlike what was currently being constructed. Different superstructure designs and increased traffic loading were not accounted for when the limit was determined.

The ASCE Committee also investigated the beginnings of live load deflection limits. They determined that vertical bridge deflections were first limited in 1871 when the specifications for the Phoenix Bridge Company limited the passage of a train traveling at 30 mph to  $1/1200$  of the span. Then in 1905 the American Railway Engineering Association (A.R.E.A) limited depth-to-span ratios for pony trusses and plate girders to  $1/10$  and  $1/12$  for rolled beams and channels, respectively. This indirectly controlled vertical deflections and accelerations. Following the ratios established by A.R.E.A., the Bureau of Public Roads specified similar ratios in 1913, which were later adopted in the first edition of A.A.S.H.O (now AASHTO) in 1924. Table 2.1 presents these historic ratios.

	Year	Trusses	Plate Girders	Rolled Beams
<b>A.R.E.A</b>	1905	$1/10$	$1/10$	$1/20$
	1907, 1911, 1915	$1/10$	$1/12$	$1/12$
	1919, 1921, 1950, 1953	$1/10$	$1/12$	$1/15$
<b>A.A.S.H.O</b>	1913, 1924	$1/10$	$1/12$	$1/20$
	1931	$1/10$	$1/15$	$1/20$
	1935, 1941, 1949, 1953	$1/10$	$1/25$	$1/25$

Table 1: Historic Depth-to-Span Ratios (ASCE, 1958)

Today's  $L/800$  limit was established in 1936 by the Bureau of Public Roads, following a study conducted to address complaints of objectionable vibration on steel highway girder bridges.

A survey was conducted in 1970 by Oehler (Oehler, 1970) that polled state bridge engineers on the effects of bridge vibration on pedestrians and vehicle passengers. Approximately 35% of the responses (out of 41) indicated that there were issues with

vibration, primarily on continuous, composite bridges. Additionally, the survey showed that only pedestrians or parked vehicles on bridges had objections to vibration, and that the limit of vibration found to be objectionable was obviously subjective and varied extensively. Oehler went on to make recommendations for the replacement of the AASHTO deflection limit on the basis of controlling bridge stiffness under three groups:

1. Bridges subject to vehicular traffic only should not have to adhere to any deflection limits. Stress restrictions shall control.
2. Bridges that allow pedestrian access and vehicle parking in urban areas should have a minimum stiffness of 200 kips/inch deflection.
3. Bridges that permit fishing benches should follow the guidelines of Group 2, and also have 7.5% critical damping.

The effect of bridge slenderness and flexibility on human response to vibration and serviceability was investigated by Wright and Walker (Wright and Walker, 1971). They concluded (and confirmed with Oehler's survey) that human response to bridge motion is a matter of comfort rather than safety. Drivers in moving vehicles are unaffected by bridge vibration, and current restrictions on flexibility do not effectively limit the dynamic component of acceleration. Additionally, they go on to state:

“Current limits on flexibility and slenderness do affect bridge economy because they may prevent economical applications of high strength steels and of slender girders. Trial designs with relaxed flexibility and slenderness limitations demonstrate that substantial economies are possible and that predicted human reactions would not be substantially greater than those observed when design is in accord with current criteria for flexibility and slenderness.”

Wright and Walker also noted that the human reaction to vibration is attributable to the peak acceleration of the dynamic component in deflection. Their study included review of past research done on the tolerable limits of acceleration on human beings, and developed criteria applicable to the majority of people. As shown in Figure 2.1, the authors determined the peak acceleration value for different girder flexibilities, and graphed them in relation to the human response limits.

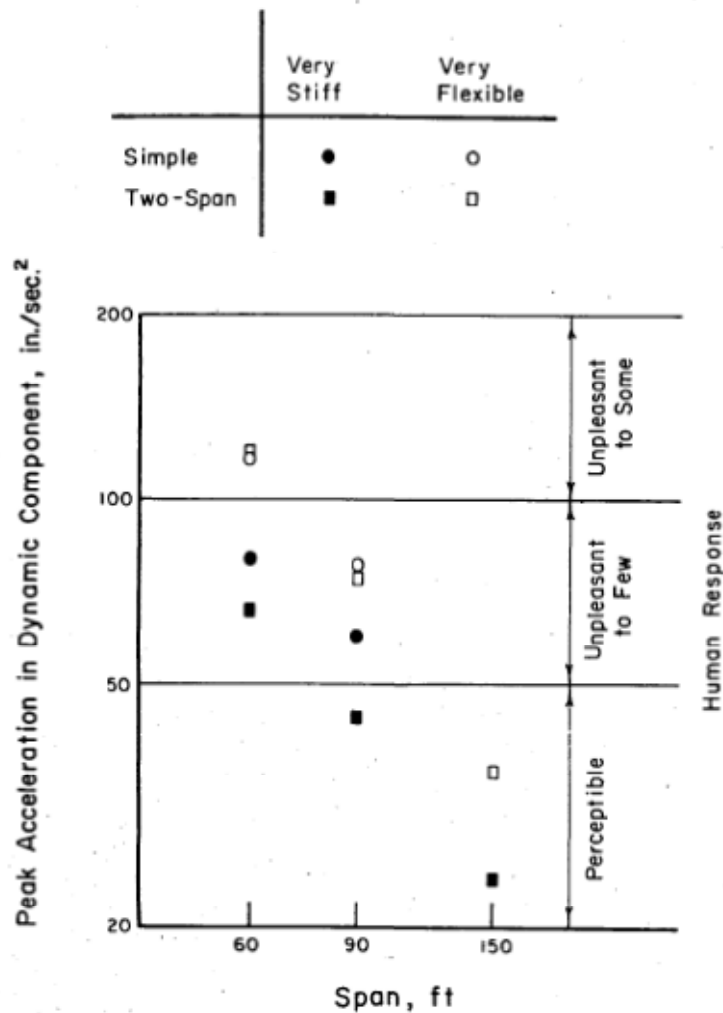


Figure 2.1: Human response to flexibility of girders (Wright and Walker, 1971)



The dynamic component of acceleration in the fundamental mode of vibration was suggested to be limited to 100 in<sup>2</sup>/sec (approximately 0.25 gravity). This was based on previous research that surveyed elevator comfort limits. Accelerations of 0.30g (116 in<sup>2</sup>/sec) for a duration of 1 to 5 seconds were noted to be unpleasant to some. However, the authors noted this limitation may still be in doubt since tolerable motions are a question of human psychology. Clearly perceptible motions do not disturb humans when they walk, dance, or ride in vehicles or elevators because the motions are anticipated. Educating pedestrians on expected bridge motions could allow this limit to be increased.

Wright and Walker also investigated the effect of bridge flexibility and deflection on deck deterioration. There are four main types of deck deterioration: spalling, surface scaling, transverse cracking, and longitudinal cracking. Reinforcement corrosion and freeze/thaw cycles of the concrete cause spalling; and scaling is caused by improper finishing and curing of the concrete. The most common form of deck deterioration, transverse cracking, is attributable to plastic shrinkage of the restrained deck, settlement around the top mat of reinforcement, long term flexure of continuous spans, and traffic induced fatigue. Longitudinal cracks occur as a result of poor mix design, temperature changes, live load effects, or a reflection of shrinkage cracking. (Wu, 2003).

The authors found no evidence to associate spalling, scaling, or longitudinal cracking to girder flexibility (i.e. deflection and vibration). Additionally, a parametric study was performed on a set of hypothetical steel girder bridges to illustrate the influence of stringer flexibility and span length on transverse moments. Since transverse deck

moments lead to tension at the top of the deck and possible deck cracking, this was of interest to the authors. Figure 2.2 shows the results of this study.

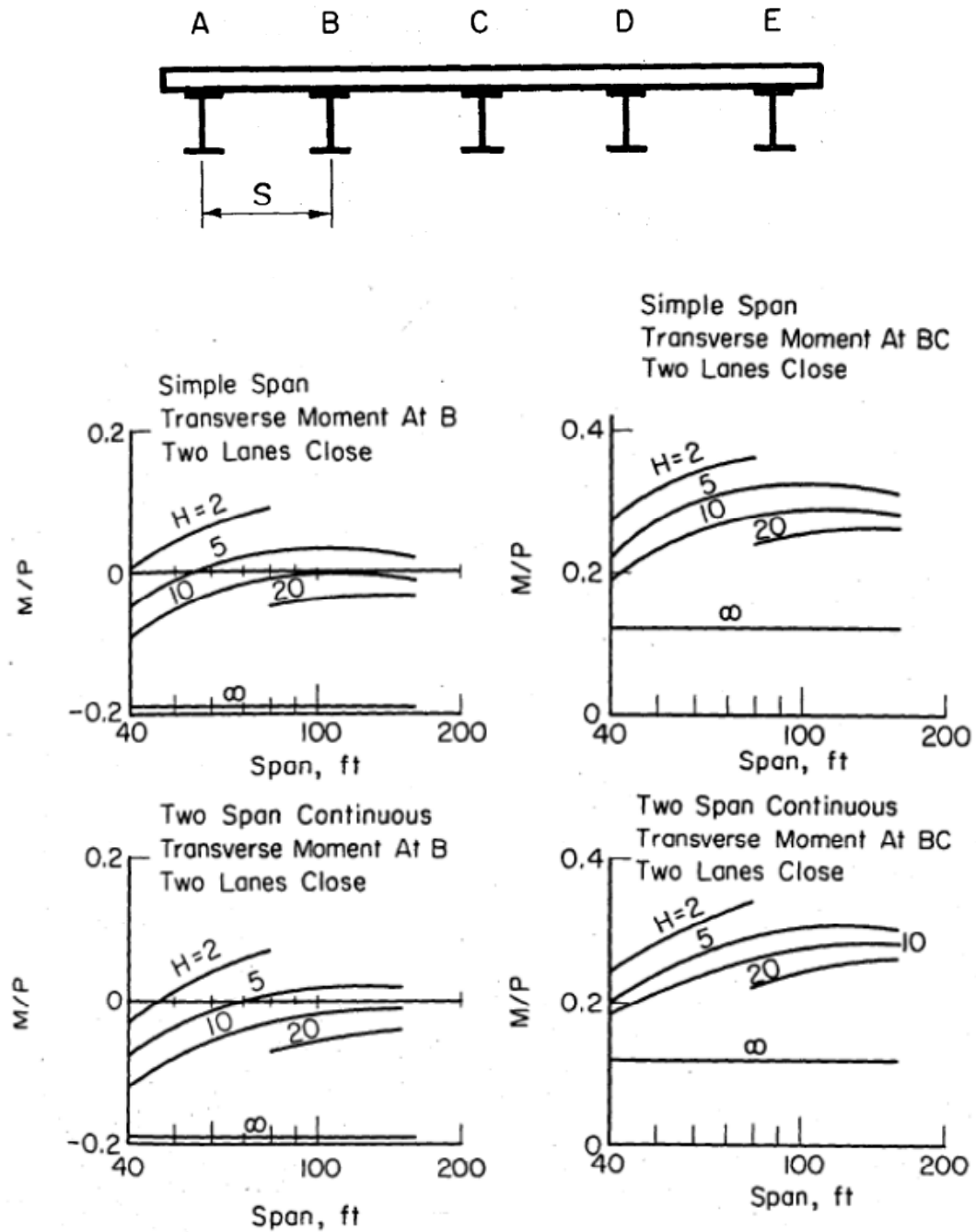


Figure 2.2: Effect of stringer flexibility of transverse moment in deck (Wright & Walker, 1971)

The curves in Figure 2.2 provide moment per unit width produced by a unit force,  $M/P$ . The stiffness parameter,  $H$ , is the ratio of the stiffness of the stringer ( $E_s, I_s$ ) and slab for the span length,  $L$ , and given as:

$$H = \frac{E_s I_s}{\frac{E_c L h^3}{12(1 - \nu)^2}}$$

Where  $E_c$ ,  $h$ , and  $\nu$  were the modulus of elasticity, thickness, and Poisson's ratio for the deck slab, respectively. The stiffness parameter  $H$  was varied between 2, 5, 10, 20, and infinity, as this range represented practical extremes of flexibility and stiffness. Span lengths were varied at 40, 80, and 160 feet for both simple and continuous spans. The graphs show that low values of  $H$  (higher girder flexibility) increased the peak positive transverse moment in the deck. At the same time, increased flexibility decreased the peak negative moments, and subsequently reduces deck cracking.

Goodpasture and Goodwin produced another study (Goodwin and Goodpasture, 1971) in 1971 which focused on the relationship between deck deterioration and live-load deflection. Twenty-seven bridges were studied to determine which type of bridges exhibited the most deck cracking. Multiple types were documented, including plate girder, rolled beams, concrete girders, prestressed girders, and trusses. Significant attention was put on continuous steel girder bridges, as they were found to exhibit the most cracking. These steel bridges were then evaluated to determine the effect of superstructure stiffness on transverse cracking. Ultimately, no correlation between girder flexibility and transverse cracking intensity could be found.

Another study (Fountain and Thunman, 1987) also supports the allegation that deflection limits show no positive effect on bridge strength, durability, safety, maintenance, or economy. They questioned the benefits of the AASHTO deflection criteria because a bridge's dynamic response changes very little as flexibility increases, due to the lateral distribution of loads to adjacent girders. Flexural stresses in the negative moment regions of continuous spans can be accurately predicted and reinforcement provided to control crack width. They recommended to modify the language in the AASHTO specification to place increased emphasis on using alternative methods to establish flexibility limits when the standard requirements have a negative impact on the economy of the design.

## **2.2 Current Research**

Recent studies have also tried to correlate excessive live-load deflections with increased structural damage or excessive vibration to no avail. A comprehensive report (Roeder, et al, 2004) performed an extensive literature review and parametric study on current live load deflection criteria. Several important conclusions were drawn from the investigation:

1. Design economies can be significantly impacted by the application of the existing AASHTO deflection limits on steel I-girder bridges made of HPS 70W steel.
2. A large number of bridges are damaged by bridge deformation, however this deformation arises from differential deflections between adjacent members, local

rotations, and deformation from bridge skew and curvature. The  $\frac{L}{800}$  limit is a poor means of controlling this deformation.

3. There are bridges that satisfy the existing deflection limits, yet provide poor vibration performance. Additionally, there are bridges which fail the existing deflection limit, yet will provide good vibration comfort and serviceability.

The authors of the study went on to recommend the eventual removal of the live-load deflection criteria from the AASHTO specifications, following the research and documentation of direct vibration frequency and amplitude controls. This would assure pedestrian and vehicle occupant comfort and structural damage control.

Boothby and Laman developed an analytical model to evaluate the cumulative damage caused by FHWA vehicle classes to concrete bridge decks (Boothby and Laman, 1999). The mechanical damage caused by live loading was compared against environmental factors to produce an expected lifetime and cost allocation program. Although their literature review found contradictions with regard to the influence of vehicle loading on bridge deck fatigue, they concluded that environmental factors play a significantly larger role in deck deterioration than does live loading.

## CHAPTER 3. GRILLAGE ANALYSIS METHOD

The three-dimensional dynamic model for the bridge-road-vehicle interaction is briefly described in this chapter. The model considers the dynamic interaction between each component through a detailed 3-D analysis.

### 3.1 Slab-On-Girder Bridge

The typical slab-on-girder bridge, as shown in Figure 3.1 can be modeled using such methods as the orthotropic plate model, semi-continuum model, finite-element model, and the grillage model. A computer program written in Fortran PowerStation on Microsoft Developer Studio and developed by Ming Liu at Bradley University will be used in this study to accurately compute maximum bridge accelerations and deflections using the grillage method (Liu, 1996). The program contains input for bridge structure geometry and cross-sectional properties, roadway roughness profiles, and vehicle loading criteria. When compiled, the three-dimensional criteria is applied to a one-dimensional assembly of transverse and longitudinal beams capable of capturing the dynamic response of the structure. The loads act in the direction perpendicular to the plane of the assembly of these beams. For a slab-on-girder bridge, the thin concrete deck spans transversely, while the girders span longitudinally between abutments.

Determining the best way to divide the bridge into grillage elements depends largely on the kind of structural behavior expected. Since the transverse elements will represent thin

slab sections with significantly smaller stiffness than the longitudinal girder elements, the number of transverse beams should be as large as possible.

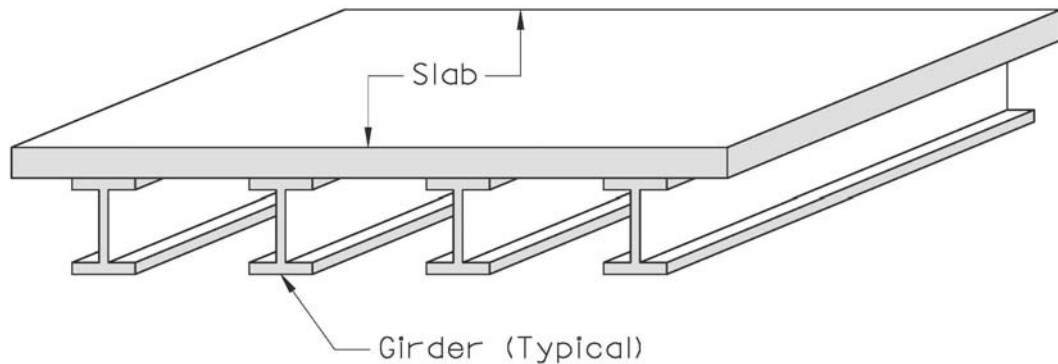


Figure 3.1: Typical Slab-on-Girder superstructure

### 3.2 Bridge Input

The grillage model reduces a three-dimensional bridge structure into a series of interconnected one-dimensional beams. The beams have flexural bending stiffness in addition to torsional stiffness. The longitudinal elements are typically placed coincident with the centerlines of the bridge girders and are assigned properties representative of a composite beam with an effective tributary slab width. If applicable, longitudinal edge elements also capture the stiffness and mass effects of a barrier parapet. Transverse elements are modeled as equivalent slab beams. Cross-frames can be modeled similar to the longitudinal girder elements, however, the majority of the transverse elements will be simple slab “panels” that have significantly less stiffness than the girders. As such, the transverse elements should be divided into as many equivalent slab beams as possible to greater capture actual load path of the structure. Figure 3.2 shows the typical cross-section properties for a grillage member.

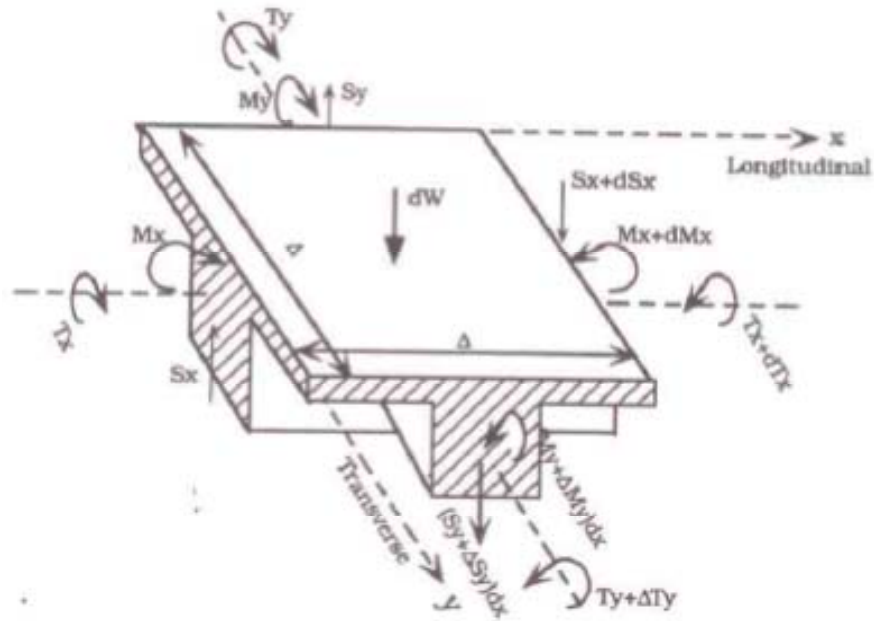


Figure 3.2: Cross-section properties for grillage member (Liu, 1996)

### 3.2.1 Longitudinal Elements

Using the concept of a composite T-beam shown in Figure 3.2, the cross section properties of longitudinal elements can be calculated using basic statics principles. The flexural bending moments of inertia are calculated about the centroids of the cross section, while using a constant centroid for interior and exterior members. Typically, it is usually convenient to place the girder spacing as the effective slab width, however, if the spacing of the girders is greater than  $1/6$  of the effective bridge span, or if the exterior overhang exceeds  $1/12$  of the effective bridge span, shear lag will significantly reduce the effective width for each girder. For structures that meet this criteria, the effective width of the slab should be the minimum of  $1/4$  of the effective bridge span, the spacing of the girders, or 12 times the slab thickness in accordance with AASHTO.



When a torque is applied to a longitudinal element, both the girder and the slab act together to resist it. Therefore, the torsional constant  $J_T$  of a longitudinal grillage member is:

$$J_T = J_g + J_{slab}$$

where  $J_g$  is the torsional constant of the girder and  $J_{slab}$  is the torsional constant of the equivalent transverse beam determined by:

$$J_{slab} = \frac{bd^3}{6}$$

where  $b$  and  $d$  are the width and thickness of the equivalent transverse beam respectively.

The torsional constant of the girder,  $J_g$ , depends on the cross sectional shape of the girder, which for a rectangular cross section is:

$$J_{gr} = \frac{3b^3d^3}{10(b^2 + d^2)}$$

where  $b$  and  $d$  are the width and height of the cross section, respectively. If  $b \geq 5d$ , then the above equation is reduced to the familiar:

$$J_{gtr} = \frac{bd^3}{3}$$

For standard shapes such as I-beams and angles,  $J_g$  can be calculated by linearly summing the individual rectangular sections of each shape.

### 3.2.2 Transverse Elements

Determining the cross sectional properties of equivalent transverse beam elements is similar to the process involved for a slab. For locations where a diaphragm exists, the

cross sectional properties are considered as the combination of the two materials and sections.

### 3.2.3 System Matrices

Using the coordinate system shown in Figure 3.2, the local stiffness matrix  $[K_L]$  for a beam, based on a combination of flexural and torsional properties with three degrees of freedom at each end is:

$$[K_L] = \frac{EI}{L^3} \cdot \begin{bmatrix} \frac{JGL^2}{EI} & 0 & 0 & -\frac{JGL^2}{EI} & 0 & 0 \\ 0 & 4L^2 & 6L & 0 & 2L^2 & -6L \\ 0 & 6L & 12 & 0 & 6L & -12 \\ -\frac{JGL^2}{EI} & 0 & 0 & \frac{JGL^2}{EI} & 0 & 0 \\ 0 & 2L^2 & 6L & 0 & 2L^2 & -6L \\ 0 & -6L & 12 & 0 & -6L & 12 \end{bmatrix}$$

where  $L$ ,  $I$ ,  $J$ ,  $E$ , and  $G$  represent length, flexural moment of inertia, torsional constant, modulus of elasticity, and shear modulus respectively. The global stiffness matrix can then be determined from an assembly of the local stiffness matrices.

Similar to the stiffness matrix, the local consistent mass matrix,  $[M_L]$  can be obtained as:

$$[M_L] = \frac{mL}{420} \cdot \begin{bmatrix} \frac{140I_0}{A} & 0 & 0 & \frac{70I_0}{A} & 0 & 0 \\ 0 & 4L^2 & 22L & 0 & -3L^2 & 13L \\ 0 & 22L & 156 & 0 & -13L^2 & 54 \\ \frac{70I_0}{A} & 0 & 0 & \frac{140I_0}{A} & 0 & 0 \\ 0 & -3L^2 & -13L & 0 & 4L^2 & -22L \\ 0 & 13L & 54 & 0 & -22L & 156 \end{bmatrix}$$

where  $m$ ,  $I_0$ , and  $A$  represent the mass per unit length of beam element, polar mass moment of inertia, and cross sectional area respectively. The global mass matrix is then obtained from an assembly of local mass matrices.

Since the local coordinate system is not always coincident with the global coordinate system, a transformation matrix must be used to assembly the local matrices into global matrices. The standard transformation matrix is expressed as:

$$[T] = \begin{bmatrix} \cos \theta & \sin \theta & 0 & 0 & 0 & 0 \\ -\sin \theta & \cos \theta & 0 & 0 & 0 & 0 \\ 0 & 0 & 1 & 0 & 0 & 0 \\ 0 & 0 & 0 & \cos \theta & \sin \theta & 0 \\ 0 & 0 & 0 & -\sin \theta & \cos \theta & 0 \\ 0 & 0 & 0 & 0 & 0 & 1 \end{bmatrix}$$

where  $\theta$  is the rotation between the local and global coordinate system.

The damping matrix,  $[C]$ , is proportional to the global mass and stiffness matrices, and can generally be expressed as:

$$[C] = [M] \sum_i a_i ([M]^{-1} [K])^i$$

where  $[M]$  is the global mass matrix,  $[K]$  is the global stiffness matrix, and  $a_i$  is an arbitrary proportionality factor. In order to determine  $a_i$ , the modal damping ratio  $\zeta_n$  for any specified mode  $n$ , must be written as:

$$\xi_n = \frac{1}{2\omega_n} \sum_i a_i \omega_n^{2i}$$

where  $\omega_n$  is the natural frequency associated with any specified mode  $n$ . The modal damping ratio can also be expressed in matrix notation as:

$$\{\xi\} = \frac{1}{2}[Q]\{a\}$$

where  $[Q]$  is a square matrix containing different powers of natural frequencies, the solution of which gives the arbitrary proportionality factors  $\{a\}$  as:

$$\{a\} = 2[Q]^{-1}\{\xi\}$$

In order to get the factors  $\{a\}$ , the modal damping ratio  $\{\zeta\}$  must first be assigned. It is necessary to estimate the modal damping ratio from previous experience such as laboratory determination or field testing of existing structures. Typical values for the modal damping ratio range from 1-2% for steel structures and 3-5% for reinforced concrete structures, with respect to the first natural frequency of the particular structure. The damping ratio for higher modes is assumed to increase in proportion to higher natural frequency.

### **3.2.4 Equivalent Nodal Loads**

Since the grillage model deals with nodal forces and displacements of an assembly of beam elements, wheel loads must be transferred into equivalent nodal forces at the intersections of the elements (node locations) when the wheel loads do not directly coincide with the grillage nodes. Additionally, stresses and displacements at any point on the bridge should be obtained from the nodal displacements using the same wheel load transformation. It is assumed that the load path of the wheel load flows from the slab to the girders, and then out to the abutments. Therefore, wheel loads are first transferred from the equivalent transverse beams to the longitudinal elements, while assuming that each transverse beam has two fixed ends acting on the longitudinal grillage members. The transformed nodal forces can be written as follows:

$$P_1 = \frac{Pd^2(2c+S)}{S^3}(2\xi^3 - 3\xi^2 + 1) + \frac{6Pcd^2}{LS^2}(\xi^2 - \xi)\operatorname{tg}\theta;$$

$$M_1 = -\frac{Pd^2(2c+S)L}{S^3}(\xi^3 - 2\xi^2 + \xi) - \frac{Pcd^2}{S^2}(3\xi^2 - 4\xi + 1)\operatorname{tg}\theta;$$

$$T_1 = -\frac{Pcd^2}{S^2}(1 - \xi);$$

$$P_2 = \frac{Pd^2(2c+S)}{S^3}(-2\xi^3 + 3\xi^2) - \frac{6Pcd^2}{LS^2}(\xi^2 - \xi)\operatorname{tg}\theta;$$

$$M_2 = -\frac{Pd^2(2c+S)L}{S^3}(\xi^3 - \xi^2) - \frac{Pcd^2}{S^2}(3\xi^2 - 2\xi)\operatorname{tg}\theta;$$

$$T_2 = -\frac{Pcd^2}{S^2}\xi;$$

$$P_3 = \frac{Pc^2(2d+S)}{S^3}(2\xi^3 - 3\xi^2 + 1) + \frac{6Pc^2d}{LS^2}(\xi^2 - \xi)\operatorname{tg}\theta;$$

$$M_3 = -\frac{Pc^2(2d+S)L}{S^3}(\xi^3 - 2\xi^2 + \xi) - \frac{Pc^2d}{S^2}(3\xi^2 - 4\xi + 1)\operatorname{tg}\theta;$$

$$T_3 = -\frac{Pc^2d}{S^2}(1 - \xi);$$

$$P_4 = \frac{Pc^2(2d+S)}{S^3}(-2\xi^3 + 3\xi^2) - \frac{6Pc^2d}{LS^2}(\xi^2 - \xi)\operatorname{tg}\theta;$$

$$M_4 = -\frac{Pc^2(2d+S)L}{S^3}(\xi^3 - \xi^2) - \frac{Pc^2d}{S^2}(3\xi^2 - 2\xi)\operatorname{tg}\theta;$$

$$T_4 = -\frac{Pc^2d}{S^2}\xi;$$

Where

$$\xi = a/L$$

Figure 3.3 below displays parameters used in the wheel load transformation.

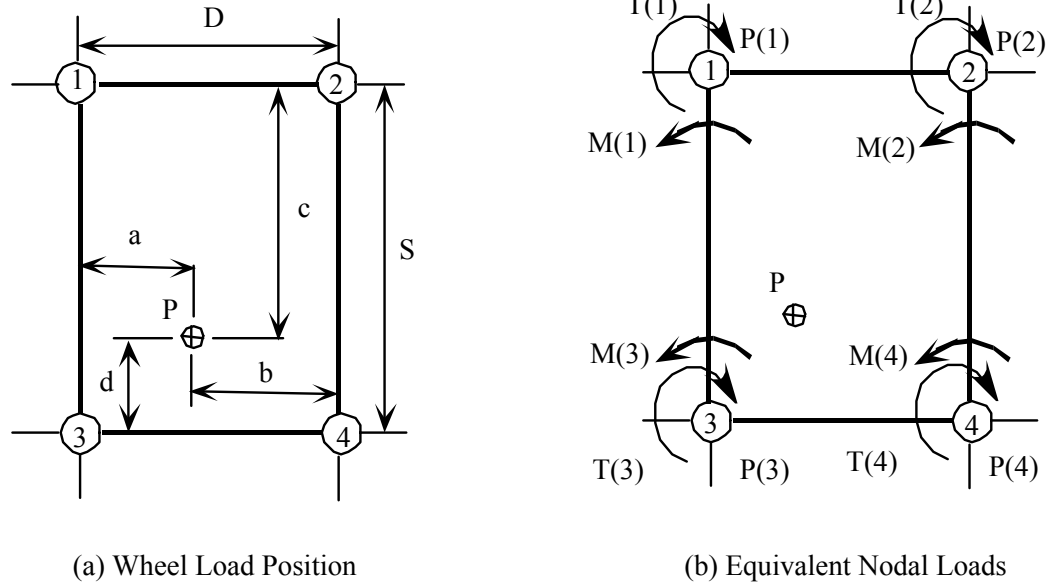


Figure 3.3: Wheel Load Transformation

### 3.2.5 Dynamic Equations

Following the input of the bridge geometry, support conditions, element flexural and torsional stiffnesses, and mass distribution, the program then assembles mass  $[M]$  and stiffness  $[K]$  matrices based on a global coordinate system. A value for damping is also input, allowing the program to assemble a damping matrix  $[C]$  and completing a full definition of the structure's dynamic attributes. The global dynamic equation for a structure subjected to wheel loads can then be created following:

$$[m]\ddot{x} + [c]\dot{x} + [k]x = [F]$$

where

$[F]$  = loading matrix

$\ddot{x}$  = acceleration matrix

$\dot{x}$  = velocity matrix

$x$  = displacement matrix

### 3.3 Road Roughness Input

Uneven finishes on bridge roadways can cause increased vehicular dynamic load effects, thereby increasing the maximum acceleration response that a structure will see. The program has the capability to model a roughness profile under each vehicle's wheel line. The profile is randomly generated using a stationary Gaussian process. The random amplitudes of the profile can be limited within ranges to create different scenarios for smooth, moderate, and severe roadway conditions. Alternatively, manual methods and high-speed profiling systems can be used to measure road roughness profiles. Liu (1996) presents a detailed description of the generation of correlated road roughness profiles.

### 3.4 Vehicle Input

Figure 3.4 shows how the program models the vehicular loading. The program uses a five-axle semi tractor-trailer for the purposes of applying load to the bridge elements. It assumes the truck is composed of three parts: tire, suspension, and truck body. The truck body and axles are represented as rigid bodies connected to non-linear springs that dissipate energy during each cycle of oscillation, i.e. a suspension system. The truck tires are modeled as linear springs with a constant stiffness, and tire damping effects are

ignored. The spring constant of the tires is assumed at 5,000 lb/in/tire based on previous research.

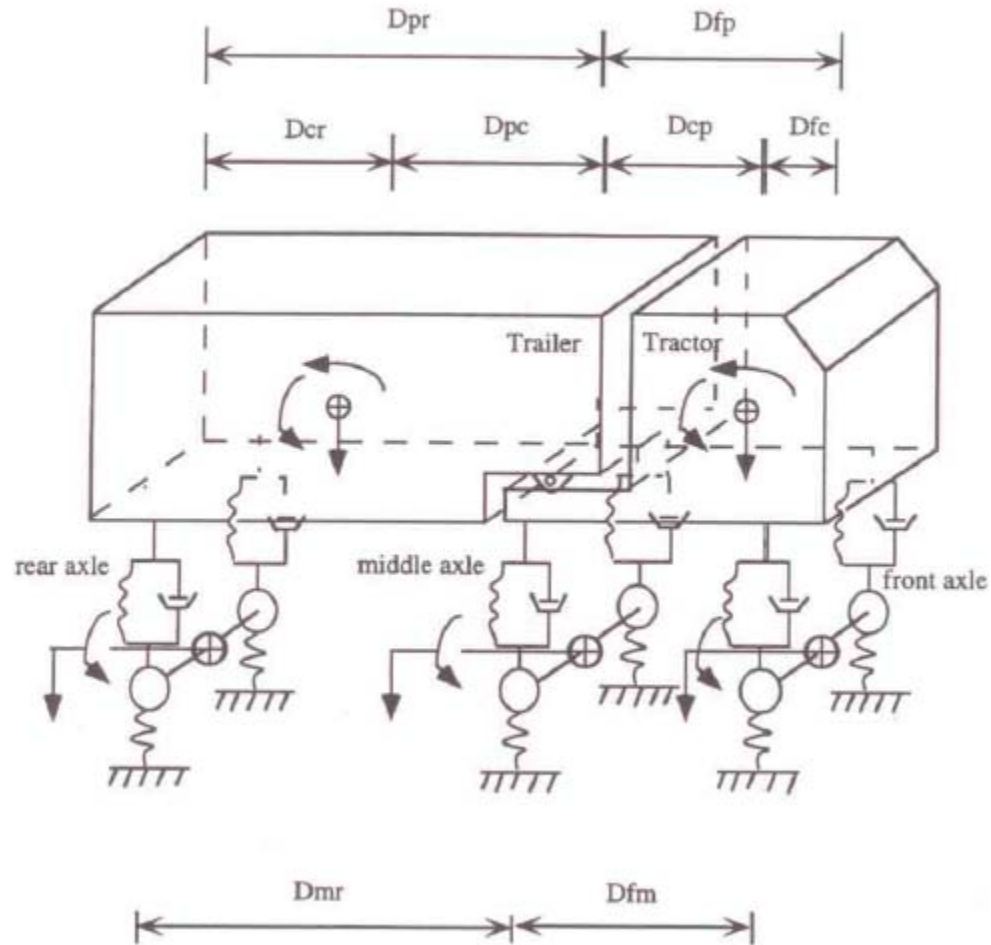


Figure 3.4: Vehicle input (Liu, 1996)

Because of the complexity of the tire-suspension mechanical properties, five assumptions are made to simplify the model:

1. Truck bodies and tire-axle sets are rigid.
2. Mass centers of the tractor and semi-trailer are assumed to be at the same level of the pivot point.



3. All of the vehicle components move with the same speed in the longitudinal direction.
4. Each tire contacts the bridge at a single point.
5. Only vertical interaction forces between the bridge and vehicle are considered (i.e. ignoring the horizontal friction forces).

The suspension system is assumed to be a multi-leaf spring suspension, which is essentially a non-linear device that dissipates energy during each cycle of oscillation. The frequency of oscillation usually occurs between 0 to 15 Hz. Previous research has shown that the force-deflection relationship of vehicle suspensions are independent of the frequencies of oscillation, but are dependent upon the amplitudes of the suspension motions and nominal applied loads. This force-deflection relationship is expressed as:

$$SF_i = SF_{ENVi} + (SF_{i-1} - SF_{ENVi})e^{-|\delta_i - \delta_{i-1}|/\beta}$$

where

$SF_i$  = suspension force at the current time step

$SF_{i-1}$  = suspension force at the last time step

$\delta_i$  = suspension deflection at the current time step

$\delta_{i-1}$  = suspension deflection at the last time step

$SF_{ENVi}$  = suspension force corresponding to the upper and lower boundaries of the envelope of the measured spring suspension characteristics at the deflection,  $\delta_i$

$\beta$  = input parameter used for describing the rate at which the suspension force

within a hysteresis loop approaches the outer boundary of the envelope

In the above equation,  $SF_{ENVi}$  and  $\beta$  have different values for the front, middle, and rear tire-axle sets based on their respective force-deflection diagrams.

The truck bodies are modeled as masses subjected to rigid body motion. The mass moments of inertia of the truck bodies are derived assuming trapezoidal and uniform weight distribution in the x-x and y-y directions as shown in Figure 3.5. The mass moment of inertia in the x-x direction,  $I_{xx}$ , can be expressed in terms of the constant mass density of the truck,  $\rho$ :

$$I_{xx} = \frac{\rho \beta^3 L(p + q)}{24}$$

and for  $I_{yy}$ :

$$I_{yy} = \frac{\rho B L^3}{36} \frac{p^2 + 4pq + q^2}{p + q}$$

where

$B$  = width of truck body

$L$  = length of truck body

$p$  and  $q$  = assumed parameters

The volume,  $V$ , and the relationship between  $p$  and  $q$  are given from the geometric properties of the trapezoidal shape:

$$V = \frac{p + q}{2} (1 + 2r)(a + b)B$$

$$q = \frac{(r + 2)a + (r - 1)b}{(r - 1)a + (r + 2)b} p$$

where

a = distance between the mass center and front axle

b = distance between the mass center and rear axle

r = c/(a+b)

c = distance between the truck body edges and axles

The dynamic equations of motion of the truck for three directions: rotation, pitch, and roll, are derived considering the equilibrium state of the tractor trailer at the pivot point. The equilibrium equations of the truck are then assembled and expressed as a [7 x 7] matrix:

$$[A]x\{\ddot{Z}\} = [B]$$

Where [A] depends on the truck geometry, body moment of inertia, and mass distribution; [B] represents the suspension forces and geometry of the truck configuration; and  $\{\ddot{Z}\}$  represents the degrees of freedom. The matrices are as shown below:

$$[A] = \begin{bmatrix} \frac{I_{T\theta}}{D_{fm}} & -\frac{I_{T\theta}}{D_{fm}} & 0 & 0 & 0 & 0 & -(a_{fc} - a_{fp})D_{fm} \\ \frac{I_{R\theta}}{D_{pr}} \left( \frac{1}{2} - a_{fp} \right) & \frac{I_{R\theta}}{D_{pr}} a_{fp} & -\frac{I_{R\theta}}{2D_{pr}} & \frac{I_{R\theta}}{2D_{pr}} & 0 & -\frac{I_{R\theta}}{2D_{pr}} & a_{pc}D_{pr} \\ \frac{I_{T\alpha}}{SD} & 0 & 0 & -\frac{I_{T\alpha}}{SD} & 0 & 0 & 0 \\ 0 & 0 & \frac{I_{R\alpha}}{SD} & 0 & 0 & -\frac{I_{R\alpha}}{SD} & 0 \\ m_T \left( \frac{1}{2} - a_{fc} \right) & m_T a_{fc} & 0 & \frac{m_T}{2} & 0 & 0 & -1 \\ m_R \left( \frac{1-a_{pc}}{2} - a_{fp}(1-a_{pc}) \right) & m_R a_{fp}(1-a_{pc}) & m_R \frac{a_{pc}}{2} & m_R \frac{(1-a_{pc})}{2} & 0 & m_R \frac{a_{pc}}{2} & 1 \\ 1 & -1 & 0 & -1 & 1 & 0 & 0 \end{bmatrix}$$

$$[B] = \begin{bmatrix} -(1-a_{fc})D_{fm}(SF_{fl} + SF_{ml}) + a_{fc}D_{fm}(SF_{fr} + SF_{fr}) \\ -(1-a_{pc})D_{pr}(SF_{rr} + SF_{rl}) \\ \frac{SD}{2}(SF_{fr} + SF_{mr} - SF_{fl} - SF_{ml}) \\ \frac{SD}{2}(SF_{rr} - SF_{rl}) \\ (SF_{fr} + SF_{mr} + SF_{fl} + SF_{ml}) \\ SF_{rr} + SF_{rl} \\ 0 \end{bmatrix}$$

$$\{\ddot{Z}\} = \begin{Bmatrix} \ddot{z}_{fsr} \\ \ddot{z}_{msr} \\ \ddot{z}_{rsr} \\ \ddot{z}_{fsl} \\ \ddot{z}_{msl} \\ \ddot{z}_{rsl} \\ P_j \end{Bmatrix}$$

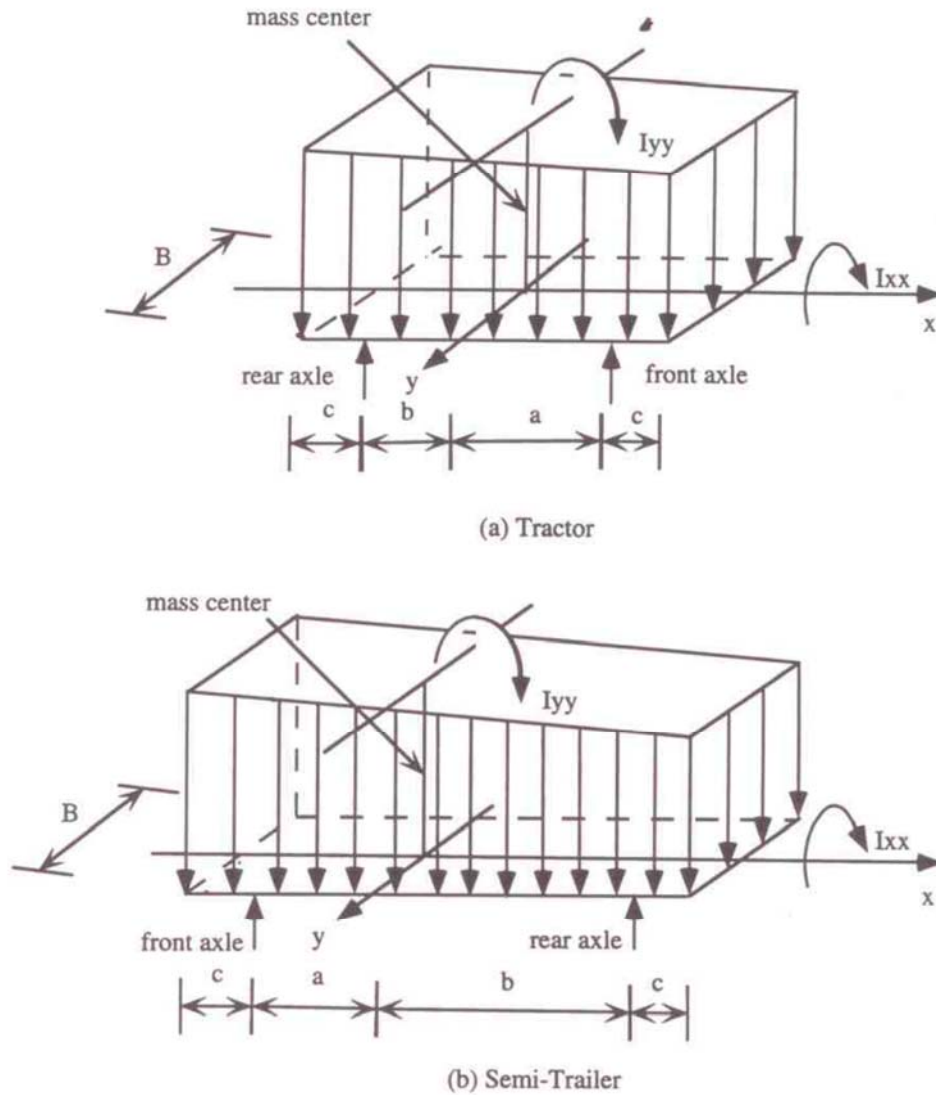


Figure 3.5: Truck mass distribution (Liu, 1996)

### 3.5 Output/Computer Processing

The computer model for grillage method includes matrix generation and decomposition, eigenvalue and eigenvector extraction from free dynamic equations of the bridge, and a step-by-step transient response, using the bridge parameters, road profiles, and truck configurations entered as the input for the program.

Newmark- $\beta$  method is used to integrate the dynamic equations of the bridge under the wheel loads. Based on the linear acceleration method, the forward integration of velocities and displacements are given as below:

$$\dot{\delta}_{t+\Delta t} = \dot{\delta}_t + [(1-\alpha)\ddot{\delta}_t + \alpha\ddot{\delta}_{t+\Delta t}]\Delta t$$

$$\delta_{t+\Delta t} = \delta_t + \dot{\delta}_t\Delta t + \left[\left(\frac{1}{2}-\beta\right)\ddot{\delta}_t + \beta\ddot{\delta}_{t+\Delta t}\right]\Delta t^2$$

where

$\alpha, \beta$  = weighing factors

In order to capture the dynamic behavior of the bridge within a reasonable accuracy, the interval between successive time increments is taken as 0.01. The simulation starts when the front axle of the truck enters the bridge, and stops when the rear axle leaves the bridge. At each time step, the wheel positions are located using truck configurations, truck speed, and time increments. The initial conditions of the current time step are the same as the computed results of the previous time step. The assumed wheel loads are transferred into the nodal loads in the grillage mesh, considering the applied forces, bending and torsional moments. When the first contact happens between the tire and the bridge, bridge stiffness and mass matrix are generated, and the bridge natural frequencies and normal modes are obtained by solving for eigenvalues and eigenvectors. The eigenproblems are solved by the Jacobi method, which is an iterative procedure that can approach the eigenvalues using a finite number of steps. Using the grillage nodal accelerations, the grillage nodal velocities and displacements are integrated by the Newmark- $\beta$  method. The bridge displacements at each wheel position are calculated

from the four adjacent nodal displacements, using displacement shape function as following:

$$v = N_1 v_0 + N_2 \theta_0 + N_3 v_L + N_4 \theta_L$$

where

$v$  = displacements at any points on the bridge

$$N_1 = 1 - 3\xi^2 + 2\xi^3$$

$$N_2 = L(\xi - 2\xi^2 + \xi^3)$$

$$N_3 = 3\xi^2 - 2\xi^3$$

$$N_4 = L(-\xi^2 + \xi^3)$$

The new wheel loads are computed from the resulting girder-deck displacements at the wheel positions and the road roughness profile. If the difference between the new and assumed wheel loads is less than the designated tolerance program will continue to the next time step. Otherwise, the program will go back to the beginning of the current time step, using the new wheel loads as the assumed wheel loads. Once the iteration converges, the girder deflections at given locations can be calculated. Similarly, strains and stresses can be obtained at any point in any girder.

## CHAPTER 4. GRILLAGE MODEL DEVELOPMENT

This chapter discusses the sample structure and details the approach used to calibrate the field testing data with the grillage model. Calibration is also performed using the finite-element modeling program, CSiBridge.

### 4.1 Sample Test Bridge

The sample structure used in this study is a single span, welded steel plate I-girder bridge with a precast panel deck and bituminous overlay. As shown in Figure 4.1, the cross-section is composed of five 7'-2" deep girders spaced at 8'-6" center-to-center with 3'-8" overhangs. The precast, post-tensioned slab panels are 8.5" thick with a 3.25" thick overlay on top. The out-to-out width of the structure is 41'-4" and it carries two 11'-9" lanes of traffic with a 9'-10" shoulder. The bridge spans 127'-4" from centerline of bearing to centerline of bearing and has five different types of girder geometry. Web thickness remains constant throughout the span at 0.5", however top and bottom flange widths and thicknesses vary throughout. The bridge spans perpendicular to the abutments and has no skew. Table 2 displays the girder section properties for the structure. A Jersey-shaped barrier parapet is present on the structure. It is 3'-6" high and 1'-6" wide at the base where it connects with the deck.



Girder Section	Web Depth (in)	Web Thickness (in)	Top Flange		Bottom Flange	
			b <sub>f</sub> (in)	t <sub>f</sub> (in)	b <sub>f</sub> (in)	t <sub>f</sub> (in)
1	86.61	0.47	18.90	0.71	18.90	0.79
2	"	"	"	0.87	18.90	0.79
3	"	"	"	0.87	25.61	0.95
4	"	"	"	1.10	25.61	0.95
5	"	"	"	1.10	25.61	1.19

Table 2: Sample structure girder dimensions (see Figure 4.3 for location)

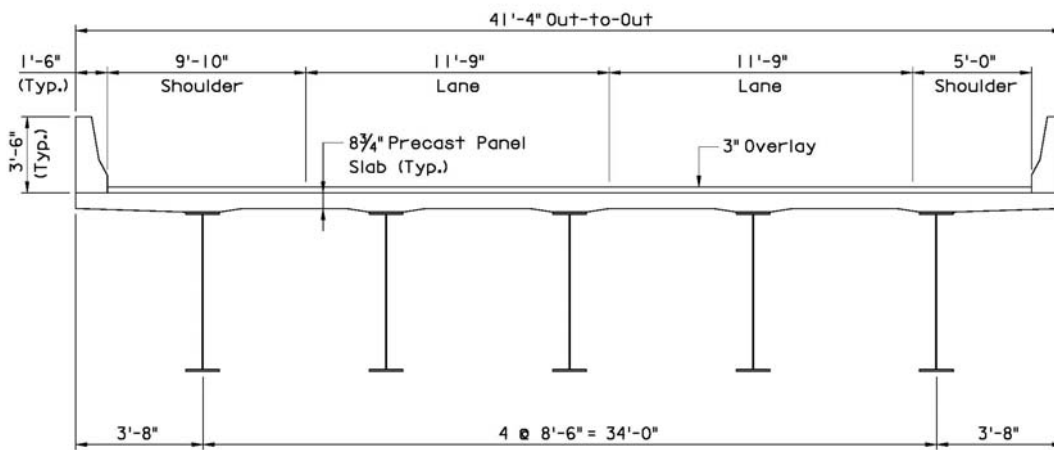


Figure 4.1: Sample structure cross-section (looking north)

Three different types of crossframes are present on the bridge. The end diaphragms, located directly along the centerline of bearing at the abutments, are 36" deep spliced plate girder sections, bolted directly to the end bearing stiffeners. The top flange of the end diaphragms are embedded in the slab. Intermediate diaphragms, spaced at 16'-5" throughout the span, alternate between a single-angle K-brace and 5'-11" deep built-up plate diaphragms. Diaphragm types and layout are shown in Figures 4.2 and 4.3.

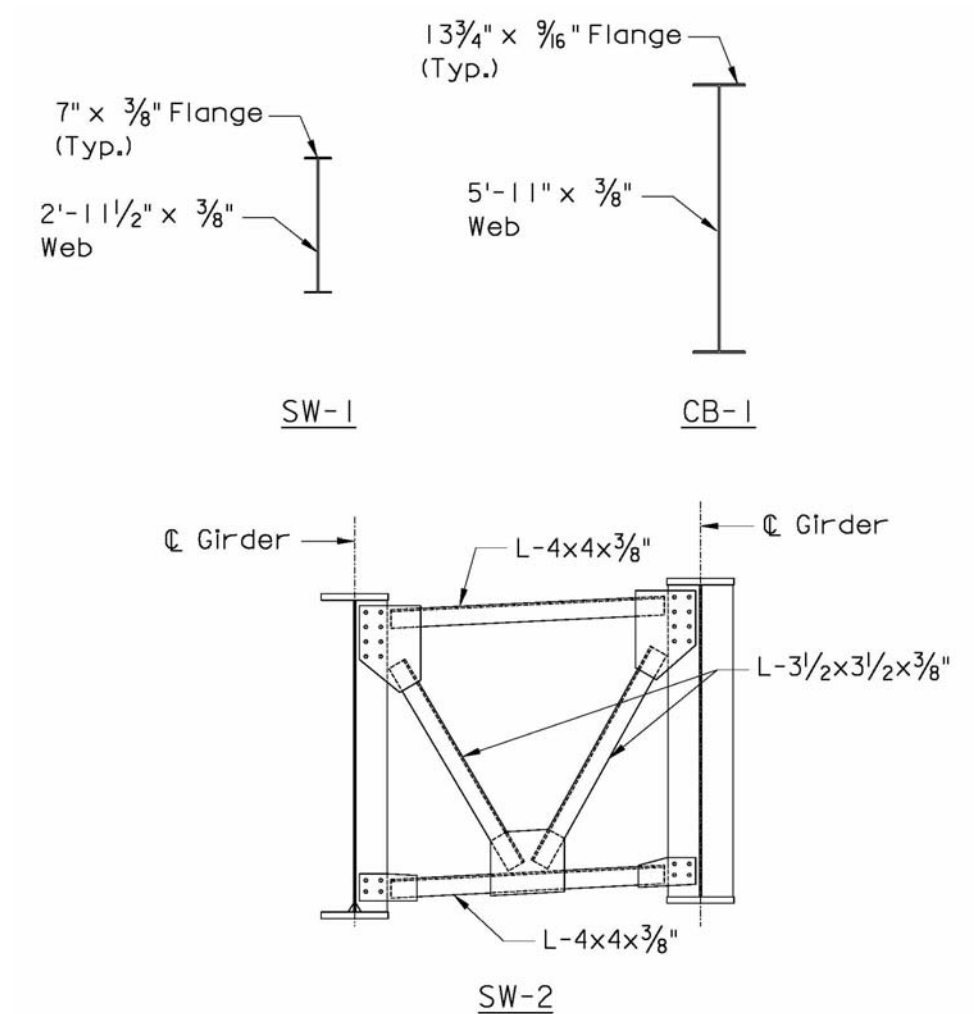


Figure 4.2: Sample structure diaphragm properties (see Figure 4.3 for location)

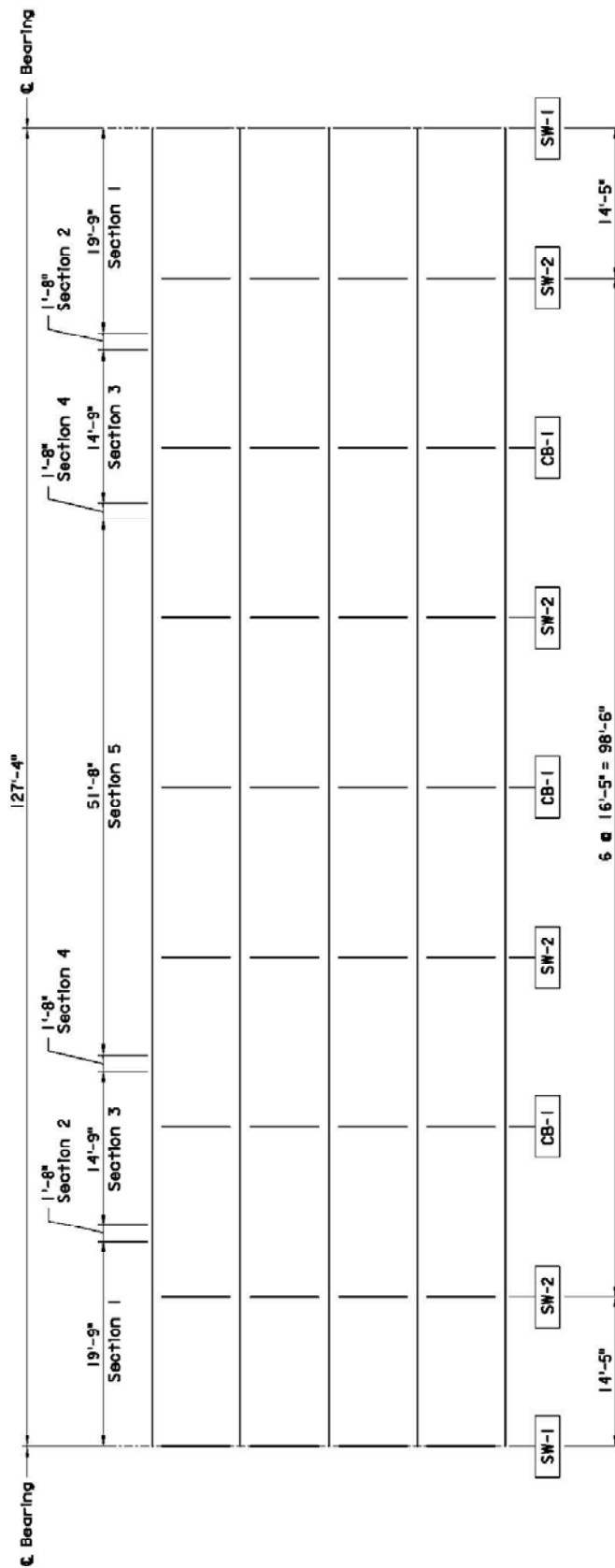


Figure 4.3: Sample structure framing plan

## 4.2 Testing Vehicle and Instrumentation Layout

Figure 4.4 presents the testing vehicle used for the field monitoring measurements. The three-axle truck has axle loads of 29.2 kips, 20.1 kips, and 20.1 kips, for a total of 69.4 kips, with axles spaced 16'-2" and 4'-5" apart. Wheel lines were spaced 6'-2" apart.

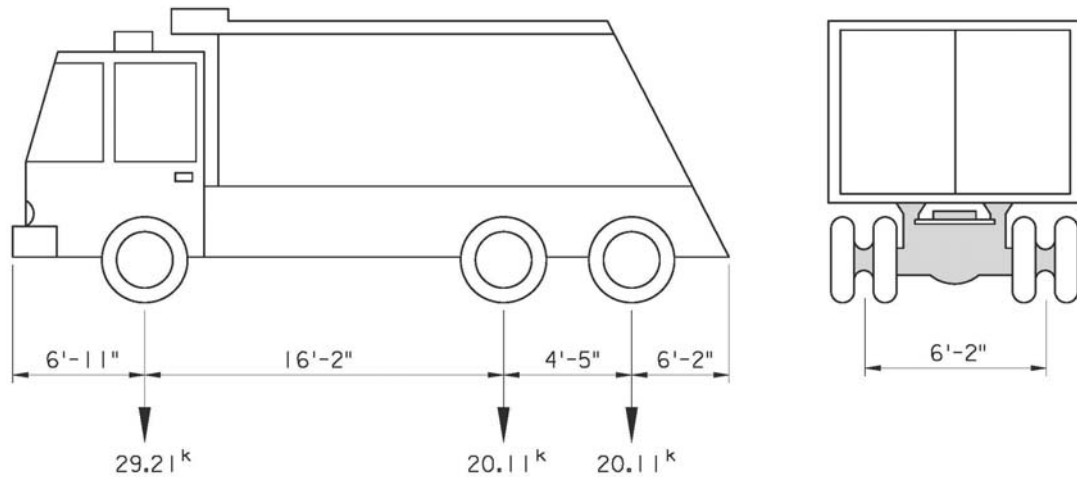


Figure 4.4: Test truck

The sensor hardware contained two Linear Variable Differential Transformers (LVDT), two accelerometers, and one laser displacement meter. A data acquisition system was also used to capture all the data simultaneously and stored on-site using a laptop computer. Figure 4.5 shows how the sensors were positioned on the bridge. For the purposes of this study, it should be noted that only the LVDT and accelerometer data will be used in the model calibration.

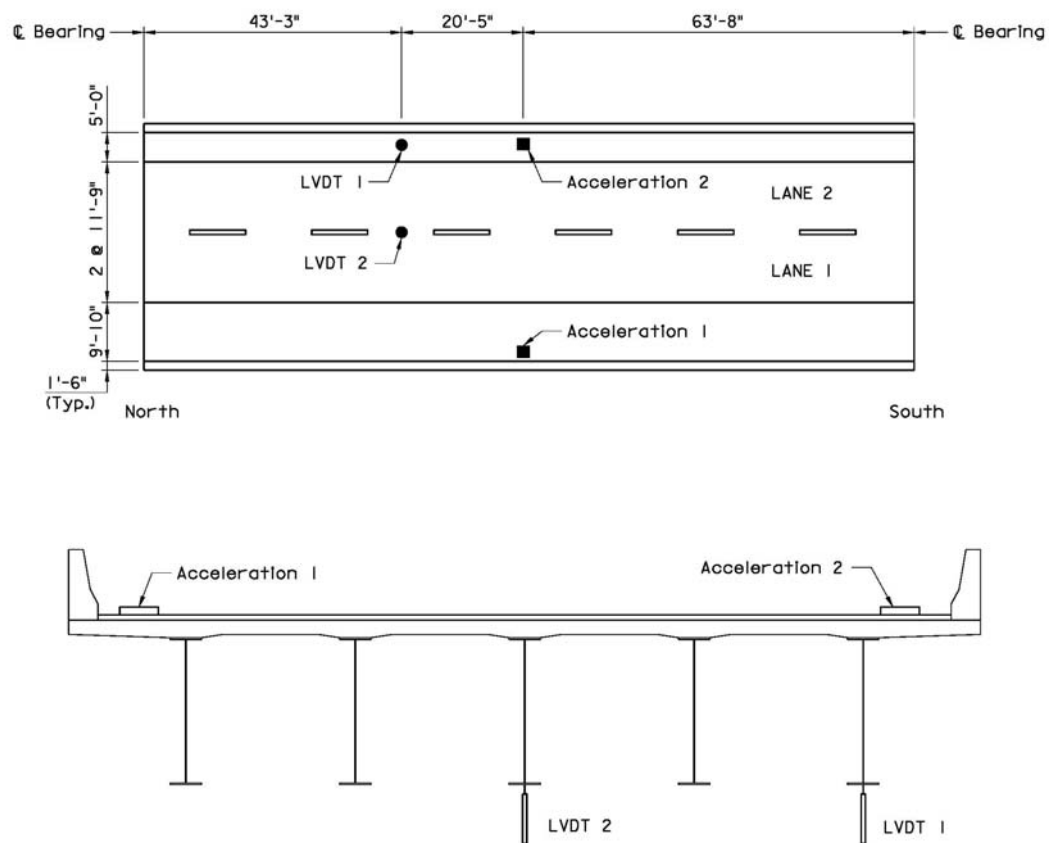


Figure 4.5: Sensor layout

The test truck was run across the bridge at three different speeds (6.2 mph, 24.9 mph, and 49.7 mph) in each lane, and in each direction for a total of twelve separate test runs as shown in Table 3.

Test No.	Lane	Speed (mph)	Direction
SS-L1-10-SB	1	6.2	Southbound
SS-L1-10-NB	1	6.2	Northbound
SS-L1-40-SB	1	24.9	Southbound
SS-L1-40-NB	1	24.9	Northbound
SS-L1-80-SB	1	49.7	Southbound
SS-L1-80-NB	1	49.7	Northbound
SS-L2-10-SB	2	6.2	Southbound
SS-L2-10-NB	2	6.2	Northbound
SS-L2-40-SB	2	24.9	Southbound
SS-L2-40-NB	2	24.9	Northbound
SS-L2-80-SB	2	49.7	Southbound
SS-L2-80-NB	2	49.7	Northbound

Table 3: Sample structure test runs

#### 4.3 Model Assumptions/Idealizations

Several assumptions were used when calibrating the grillage model with the test data:

1. No information was taken in the field as to the exact position of the test truck in the lane for each run. The truck was assumed to be located at the center of each lane. Additionally, the model started the truck movement approximately 100 inches behind the start of the bridge. This was to allow the vehicle's suspension system to fully develop its dynamic response.
2. It's a well-known fact that a bridge's barrier parapet increases the stiffness of the superstructure and plays a role in reducing bridge deflections. For this model, the barrier mass and stiffness was linearly added to the exterior girder's mass and

stiffness. This approach is reasonable considering the relatively wide girder spacing (8'-6"), any effects on the first interior girder would be negligible.

3. The overlay thickness was included as part of the deck's mass and stiffness. From a mass perspective, this assumption is valid. However, assuming the overlay is fully composite with the precast deck panels could be considered disputable. Based on preliminary model trial runs, there is definitely some degree of composite action between the deck and overlay. Implementing this assumption into the model increased the accuracy of the results, and will therefore remain.
4. In an effort to limit the amount of modeling required, only the test runs for the Southbound direction (in Lanes 1 and 2) were used for calibration purposes. It was assumed running the truck in the opposite direction would produce very similar results due to the symmetry of the structure.
5. The grillage program cannot model a K-brace diaphragm due to its inherent 2-D idealization of superstructure elements. An equivalent section was assumed with identical mass and stiffness based on a truss analysis of the diaphragm.
6. Limited details were provided for how the precast deck panels were connected to the girders. It was assumed shear stud pockets were provided and grouted during construction, effectively making the section composite. The model assumes 100% composite action between the slab and girders.
7. The structure was assumed to have 6% damping.

#### 4.4 Model Input

Dividing the structure into a series of elements and nodes, and then assigning structural properties to each element was perhaps the most difficult and tedious exercise in this study. Due to the varying girder geometry, a significant number of elements needed to be created to capture the effects of the changing mass and stiffness throughout the span. Additionally, a general requirement for grillage modeling is to partition longitudinal elements into lengths no longer than 1.5 times the longest transverse element. Figure 4.6 displays this condition. Since the slab has only a fraction of the bending stiffness of the girders, the slab flexes in the transverse direction with much greater curvature than in the longitudinal direction. Increasing the number of transverse elements helps to better demonstrate this action, as the slab will behave similar to a large number of transverse spanning planks. Elements were refined even further in areas near sensors, so as to increase the model's real-world flexural action. Figure 4.7 and 4.8 show the element and node labeling respectively for the area around the LVDT 1 sensor.

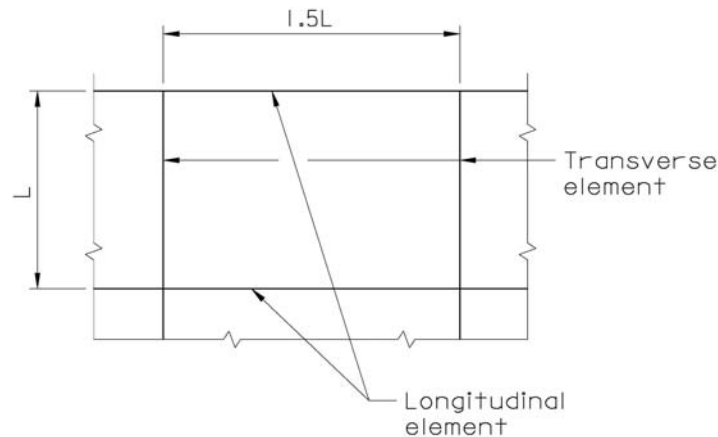


Figure 4.6: Grillage element division guideline



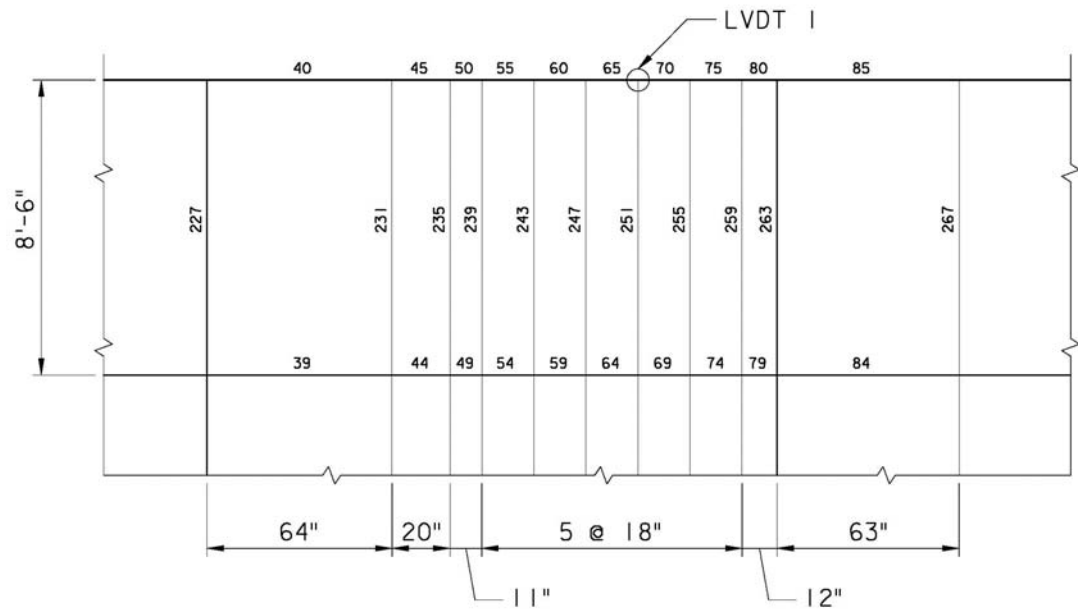


Figure 4.7: Localized area around LVDT 1 showing element division and labels

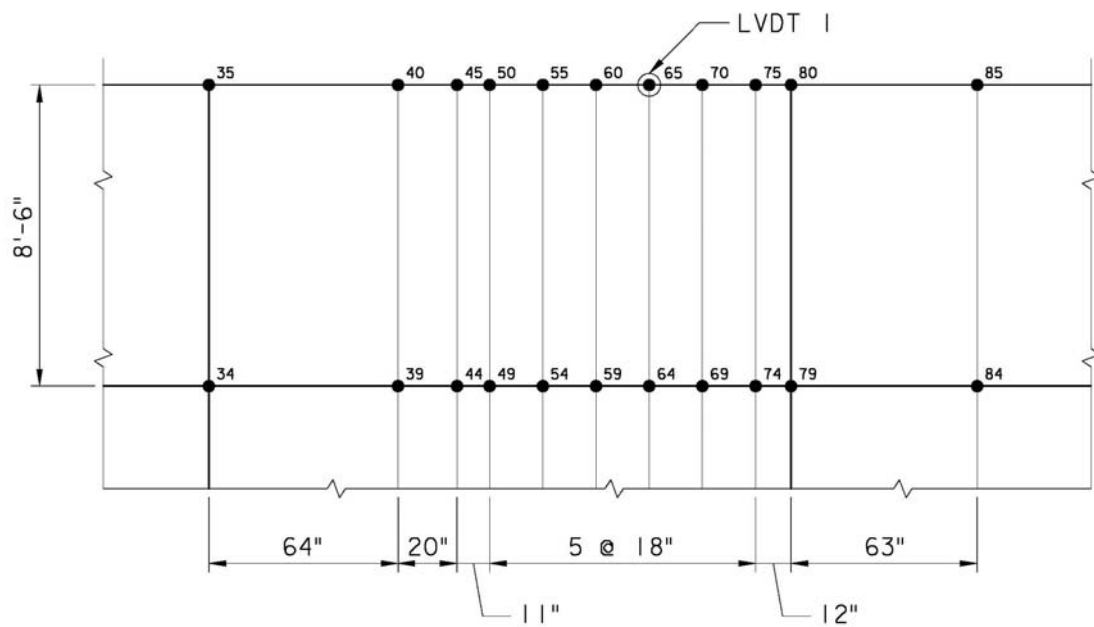


Figure 4.8: Localized area around LVDT 1 showing node labels

Each element requires four inputs: flexural moment of inertia, torsional moment of inertia, mass moment of inertia, and mass per unit area (mass distribution). The flexural and torsional moments of inertia are straightforward calculations based on the geometry of the equivalent composite section. All concrete sections were converted into equivalent steel sections using a modular ratio of approximately seven. The flexural (I) and torsional (J) moments of inertia can be calculated for a slab element using the equations:

$$I = \frac{bd^3}{12} \quad \text{and} \quad J = \frac{bd^3}{6}$$

Where b and d represent the width and thickness respectively of the equivalent transformed section.

The mass moment of inertia (IM) is a critical property to accurately model the dynamic properties of the structure. Analogous to the area moment of inertia, it characterizes an object's ability to resist bending and is needed to calculate displacement and acceleration. On a per length basis, it can be represented by the formula:

$$IM = r^2m$$

Where  $r^2$  is the radius of gyration and m is the density of the material.

Lastly, the mass distribution is simply the cross-sectional area of the section times the density of the material to generate a value of mass/unit length.

#### 4.5 Calibration Results

The model produced results very close to the measured field data, particularly with the higher speed test (49.7 mph). Since acceleration test data was not supplied for this study, only the deflection values could be compared to the modeled results, which are presented graphically in Figures 4.9 and 4.10.

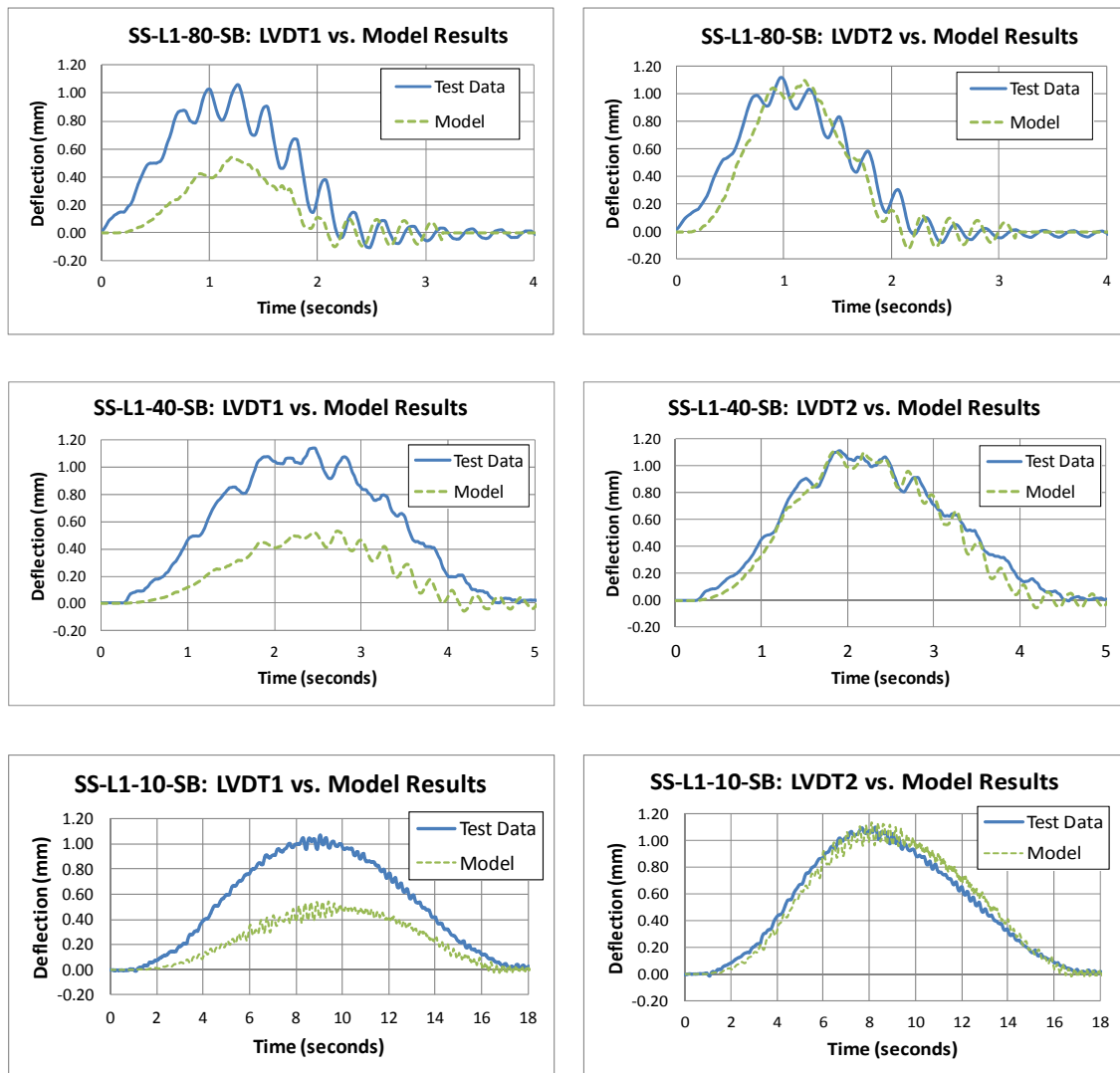


Figure 4.9: Lane 1 Southbound Deflection Results

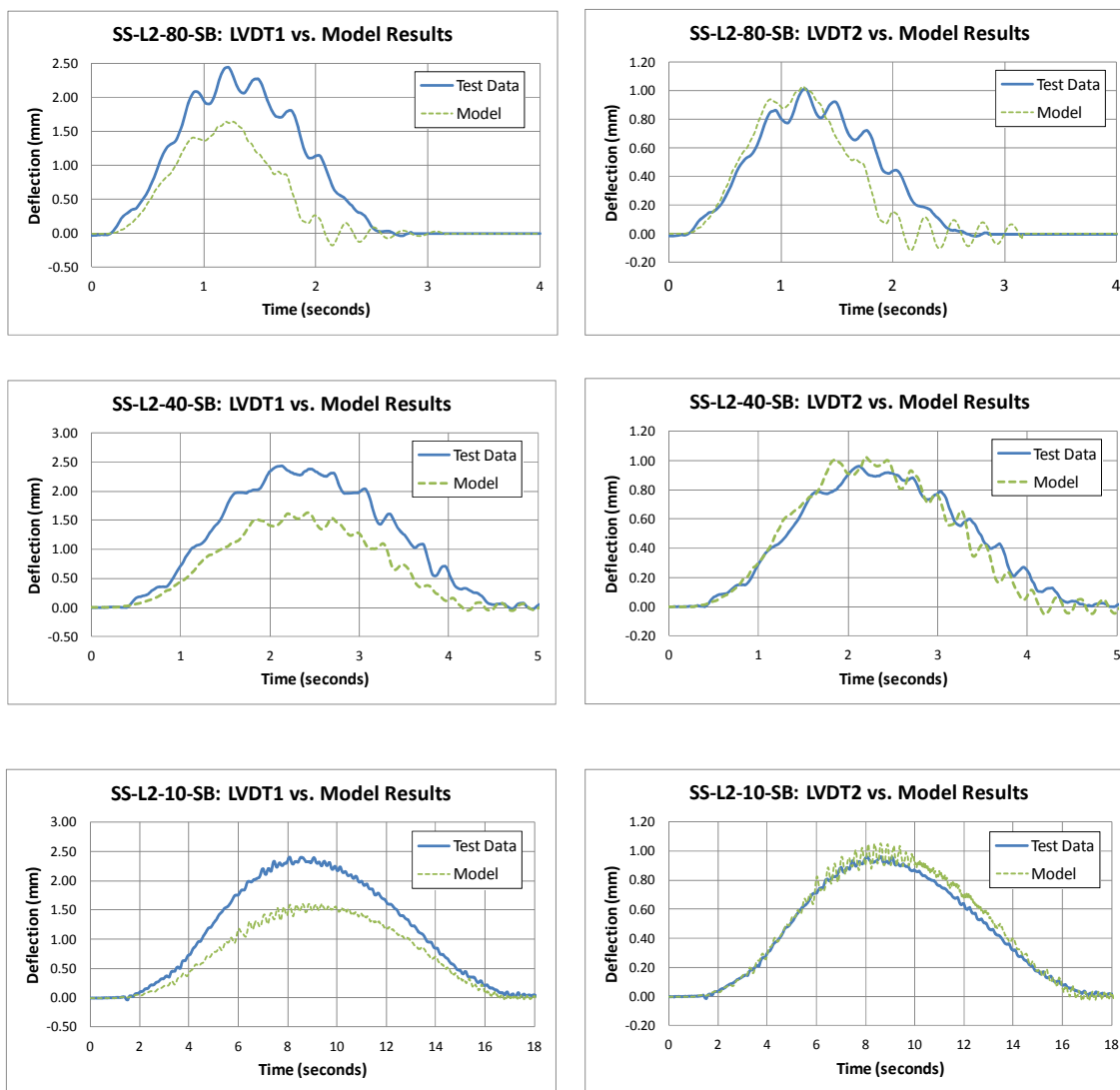


Figure 4.10: Lane 2 Southbound Deflection Results

A summary of the results is presented below in Table 4.

	Test Case	LVDT2 (mm)	LVDT1 (mm)	Accel 1 (cm/s <sup>2</sup> )	Accel 2 (cm/s <sup>2</sup> )
Lane 1 Southbound	<b>SS-L1-80-SB</b>	<b>1.114</b>	<b>1.064</b>	<b>20.16</b>	<b>15.70</b>
	<i>Model</i>	1.098	0.542	23.65	17.56
	Difference	-1%	-49%	17%	12%
	<b>SS-L1-40-SB</b>	<b>1.105</b>	<b>1.140</b>	<b>8.25</b>	<b>6.35</b>
	<i>Model</i>	1.116	0.530	13.12	8.19
	Difference	1%	-54%	59%	29%
	<b>SS-L1-10-SB</b>	<b>1.094</b>	<b>1.067</b>	<b>4.78</b>	<b>4.07</b>
	<i>Model</i>	1.137	0.544	11.76	9.75
	Difference	4%	-49%	146%	140%
Lane 2 Southbound	<b>SS-L2-80-SB</b>	<b>0.843</b>	<b>2.047</b>	<b>13.04</b>	<b>15.04</b>
	<i>Model</i>	1.032	1.646	10.82	21.91
	Difference	22%	-20%	-17%	46%
	<b>SS-L2-40-SB</b>	<b>0.952</b>	<b>2.448</b>	<b>7.43</b>	<b>16.35</b>
	<i>Model</i>	1.023	1.635	5.88	16.27
	Difference	7%	-33%	-21%	-1%
	<b>SS-L2-10-SB</b>	<b>0.955</b>	<b>2.406</b>	<b>4.12</b>	<b>6.12</b>
	<i>Model</i>	1.051	1.609	7.90	9.90
	Difference	10%	-33%	92%	62%

Table 4: Summary of model calibration results

A few things should be noted regarding the results:

1. Sensor LVDT-2 produced much closer results to sensor LVDT-1 for all test cases.

This could be due to the effect of the barrier parapet on the exterior element's stiffness. However, while the percentage difference in sensor LVDT-1 seems to be large (greater than 50% in some cases), it is important to notice the difference is on the order of less than one millimeter. Calibrating a model to this level of accuracy is excessive and not practical for the purposes of this study. Furthermore, as discussed in the following section, the model was also validated using a FEM model for deflection and found to be in agreement with the reported values.

2. Acceleration values for the 6.2 mph truck did not closely match the model's values. This will be viewed as acceptable when analyzing the entire set of results.

The goal of this paper is to investigate the effects of live load vibration. A truck moving 6.2 mph is not likely to generate excessive vibrations worth studying. While providing a somewhat useful data point, the author places a higher importance on calibrating the model with the faster test trucks. Additionally, as mentioned above, the magnitude of difference between the actual and modeled values is not very high. For example, in case SS-L1-10-SB for sensor Accel 1, a difference of  $6.98 \text{ cm/s}^2$  produces an error of 146%. While this may seem like a lot, the value is actually negligible when compared to the noticeable human vibration limit of  $127 \text{ cm/s}^2$ .

#### 4.6 FEM Calibration

An additional calibration check was done using the finite-element program CSiBridge. This program allows for the rapid creation and loading of a typical bridge structure. Deflections were checked at locations that coincided with the sensor installation points and found to be within  $\pm 0.2$  millimeters of the actual test values. Figures 4.11 and 4.12 show the model layout, which utilized shell elements for the slab, and frame elements for the girders, crossframes, and barrier. The barrier section was attached to the superstructure using a series of rigid links.

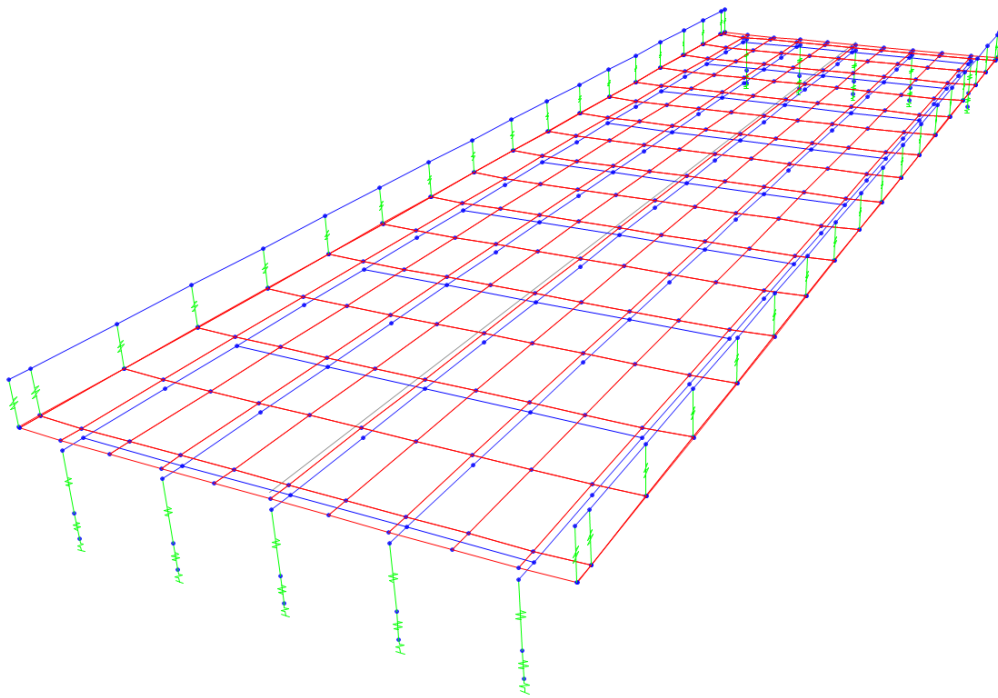


Figure 4.11: Spline view of FEM model showing shell and frame elements

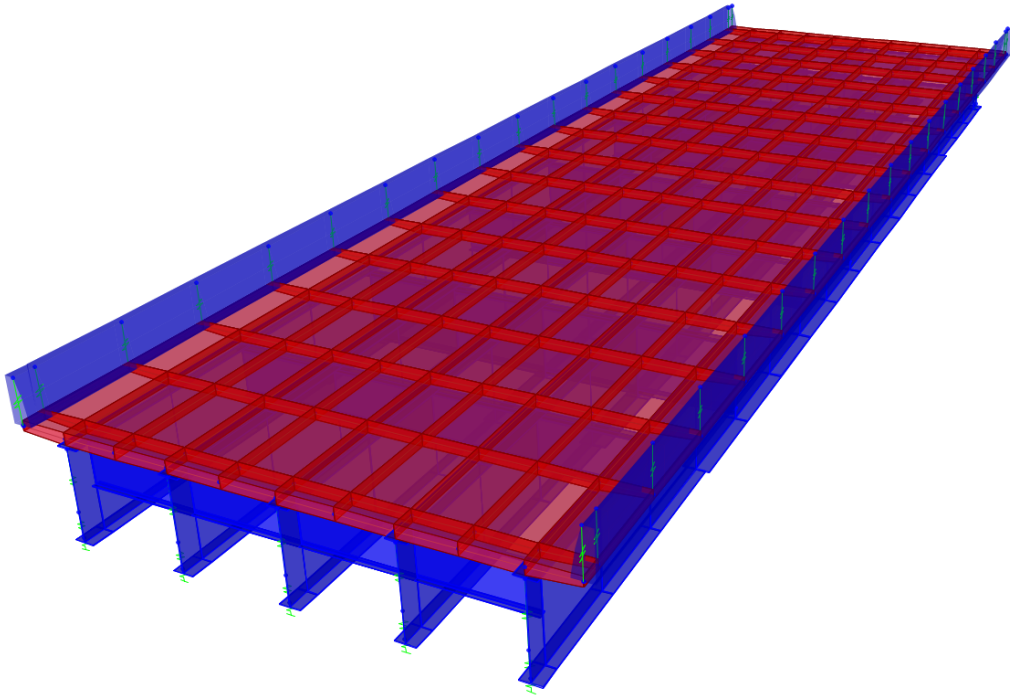
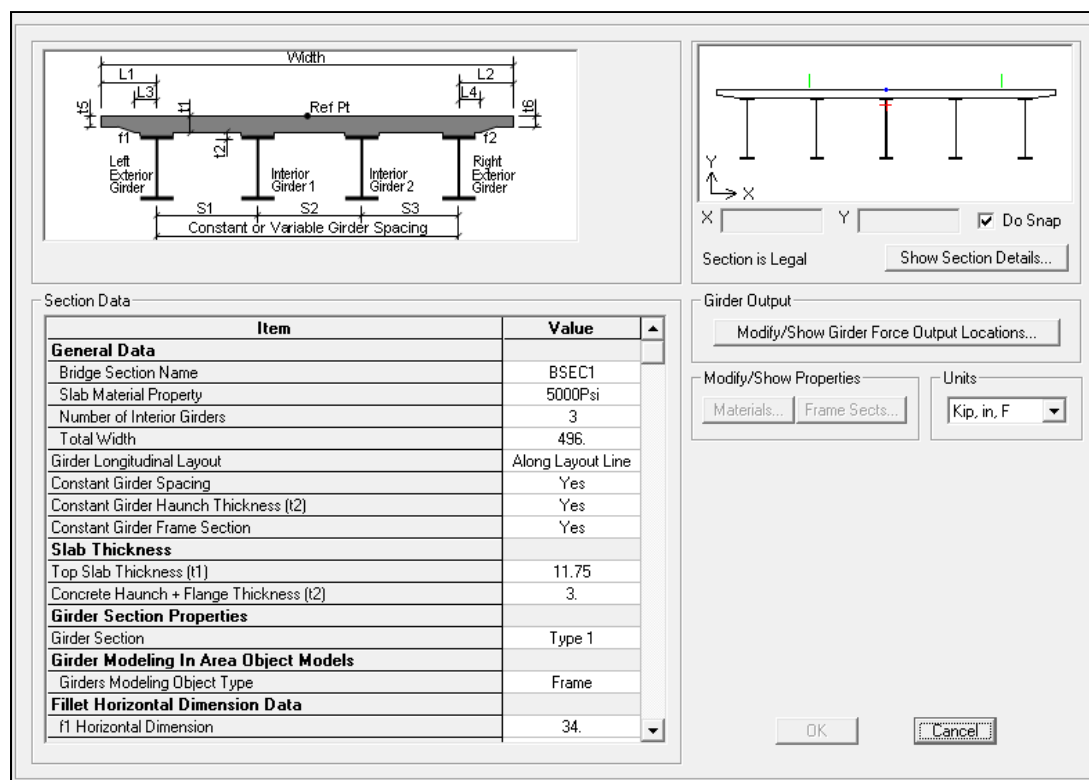


Figure 4.12: Extruded view of FEM model

Similar to the grillage program, modeling begins with entering standard bridge geometric information including: span length, number of girders, deck width and thickness, and girder spacing. Cross-section properties are then defined for all frame elements. Multiple girder cross-sections were created to model the varying stiffness throughout the span, and then manually assigned to frame elements representing that particular cross-section's location. Diaphragm properties were also imported (K-braces) and manually defined (built-up plate sections). The general input form is shown in Figure 4.13.





The figure shows the CSiBridge Deck Section Input Form. At the top left is a cross-section diagram of a bridge deck with labels for dimensions (L1, L2, L3, L4, S1, S2, S3, Width, f1, t2, Ref Pt) and girder types (Left Exterior Girder, Interior Girder 1, Interior Girder 2, Right Exterior Girder). To the right of the diagram is a small schematic of the deck layout with a coordinate system (X, Y) and a 'Do Snap' checkbox. Below the diagram is a 'Section Data' table. To the right of the table are buttons for 'Girder Output' and 'Modify/Show Properties', along with a 'Units' dropdown menu. At the bottom right are 'OK' and 'Cancel' buttons.

Item	Value
<b>General Data</b>	
Bridge Section Name	BSEC1
Slab Material Property	5000Psi
Number of Interior Girders	3
Total Width	496.
Girder Longitudinal Layout	Along Layout Line
Constant Girder Spacing	Yes
Constant Girder Haunch Thickness (t2)	Yes
Constant Girder Frame Section	Yes
<b>Slab Thickness</b>	
Top Slab Thickness (t1)	11.75
Concrete Haunch + Flange Thickness (t2)	3.
<b>Girder Section Properties</b>	
Girder Section	Type 1
<b>Girder Modeling In Area Object Models</b>	
Girders Modeling Object Type	Frame
<b>Fillet Horizontal Dimension Data</b>	
f1 Horizontal Dimension	34.

Figure 4.13: CSiBridge Deck Section Input Form

The barrier section also had to be manually defined, as shown in Figure 4.14. The geometric shape was drawn in the program and section properties were automatically computed. Since the section was modeled as a frame element, it was critical to place the connecting nodes at the centroid of the barrier section. Additionally, the barrier was attached to the deck using a series of rigid links. This assumption is valid considering that the barrier contributes to the superstructure stiffness and reinforcing bars are present that are continuous between the deck and barrier. Figure 4.15 displays the modeling assumptions used with the barrier.

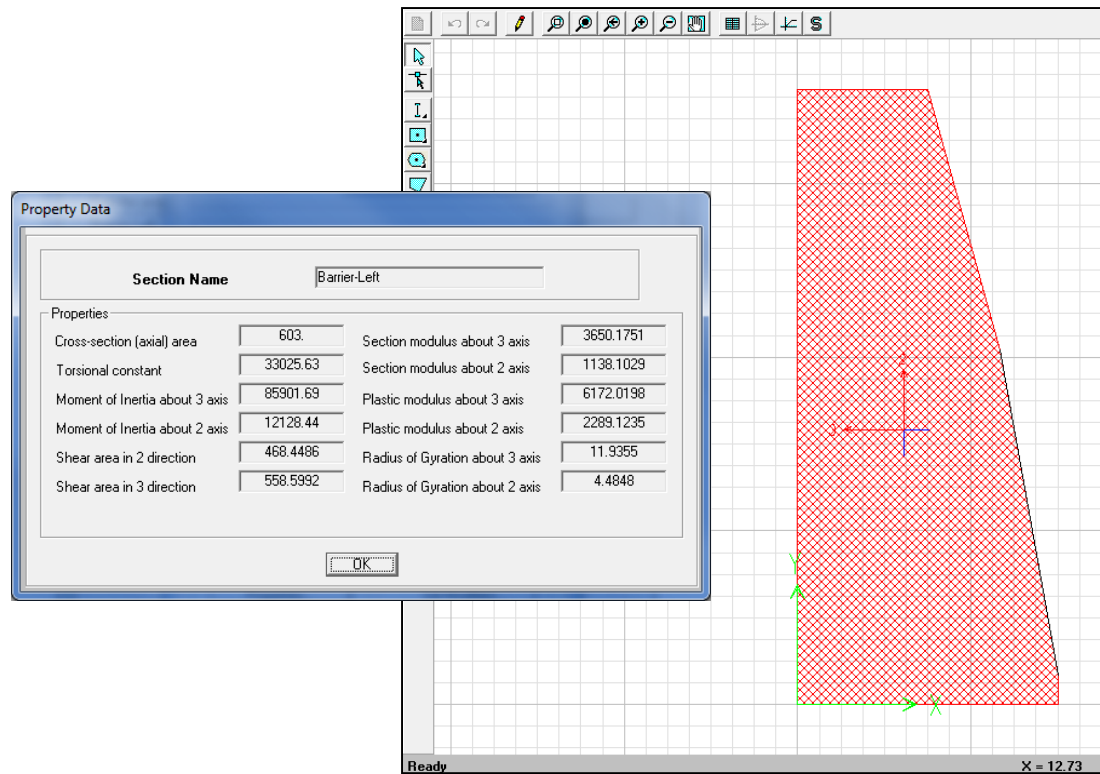


Figure 4.14: Barrier section and structural properties

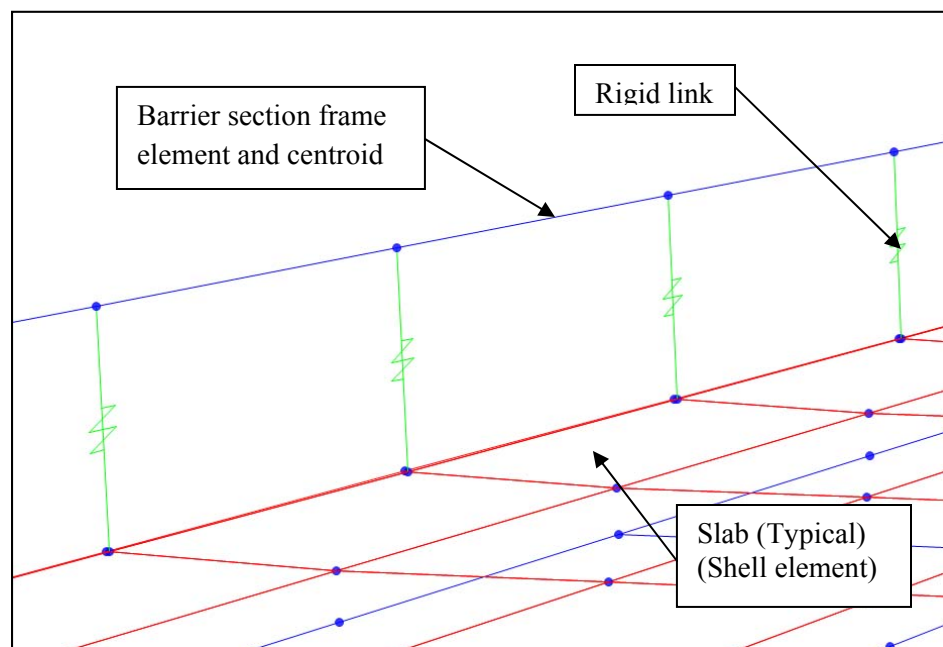


Figure 4.15: Barrier model assumptions

In order to model the composite behavior between the deck and girders, the program contains special constraint functions which are used to enforce certain types of rigid-body behavior between adjacent nodes. Composite beam action requires that a “body” constraint be used between the slab and beam nodes, which the program will automatically generate. Upon application of the body constraint, the nodes will translate and rotate together as if connected by rigid links. Additionally, computation effort is reduced as the nodes will contain their own local coordinate system, thereby lowering the number of equations to be solved in the system. The constraint equations relate the displacements at any two constrained joints (subscripts  $i$  and  $j$ ) for a body constraint. These equations are expressed in terms of the translations ( $u_1$ ,  $u_2$ , and  $u_3$ ), the rotations ( $r_1$ ,  $r_2$ , and  $r_3$ ), and the coordinates ( $x_1$ ,  $x_2$ , and  $x_3$ ) taken in the constraint local coordinate system:

$$u_{1j} = u_{1i} + r_{2i}\Delta x_3 - r_{3i}\Delta x_2$$

$$u_{2j} = u_{2i} + r_{3i}\Delta x_1 - r_{1i}\Delta x_3$$

$$u_{3j} = u_{3i} + r_{1i}\Delta x_2 - r_{2i}\Delta x_1$$

$$r_{1i} = r_{1j}$$

$$r_{2i} = r_{2j}$$

$$r_{3i} = r_{3j}$$

where  $\Delta x_1 = x_{1j} - x_{1i}$ ,  $\Delta x_2 = x_{2j} - x_{2i}$ , and  $\Delta x_3 = x_{3j} - x_{3i}$

After the program has generated the structure geometry, cross-section properties, and constraints, loading must be defined. The test vehicle was input into the program as a general vehicle shown in Figure 4.16. All vehicle live loads represent weight and are

assumed to act downward, in the  $-Z$  global coordinate direction. Longitudinally, the vehicle consists of three axle loads, each acting as a point load at a single longitudinal location along the vehicle. The width of each axle load is independently specified, which is fixed at 74 inches.

Vehicle name: Test Vehicle

Units: Kip, in, F

Floating Axle Loads

	Value	Width Type	Axle Width
For Lane Moments	0.	One Point	
For Other Responses	0.	One Point	

☐ Double the Lane Moment Load when Calculating Negative Span Moments

Usage

☒ Lane Negative Moments at Supports

☒ Interior Vertical Support Forces

☒ All other Responses

Min Dist Allowed From Axle Load

Lane Exterior Edge: 12.

Lane Interior Edge: 24.

Length Effects

Axle: None

Uniform: None

Loads

Load Length Type	Minimum Distance	Maximum Distance	Uniform Load	Uniform Width Type	Uniform Width	Axle Load	Axle Width Type	Axle Width
Fixed Length	1.		0.	Zero Width		29.21	Two Points	74.
Fixed Length	1		0.	Zero Width		29.21	Two Points	74.
Fixed Length	195.11		0.	Zero Width		20.11	Two Points	74.
Fixed Length	53.76		0.	Zero Width		20.11	Two Points	74.

Add Insert Modify Delete

☐ Vehicle Applies To Straddle (Adjacent) Lanes Only

☐ Vehicle Remains Fully In Lane (In Lane Longitudinal Direction)

Straddle Reduction Factor:

OK Cancel

Figure 4.16: Test vehicle input

Lanes are also defined on the model, transversely spaced across the deck, on which the vehicle live load is considered to act. The lanes were defined based on an eccentricity to the model's reference line, and given a width of 11.75 feet. The model then analyzes the structure by moving the vehicle along the length of the lane, with the vehicle traveling forward until the back of the vehicle exits the lane, allowing all locations to be considered. Using the model's corresponding influence lines, the maximum and

minimum values of a response quantity are then computed. Concentrated loads (wheel loads) are multiplied by the influence value at the point of application to obtain the corresponding response. The vehicle is applied as a multi-step static load case, which produces a separate linear static solution for each time step, starting at time zero. Each solution is independent, representing the displacement and stress state in the structure for the current position of the vehicle. Due to this type of analysis, the speed of the vehicle has no effect on the results. Therefore, it was most prudent to compare the values obtained from the finite-element modeling to the case where the test vehicle was traveling at 6.2 mph. This speed is assumed to be slow enough such that a linear static analysis would be acceptable. Figure 4.17 below displays the nodal deflection at the LVDT1 sensor location, which was computed to be -1.09 mm. This compared nicely with the actual test values for this location, which were measure at -1.06 mm.

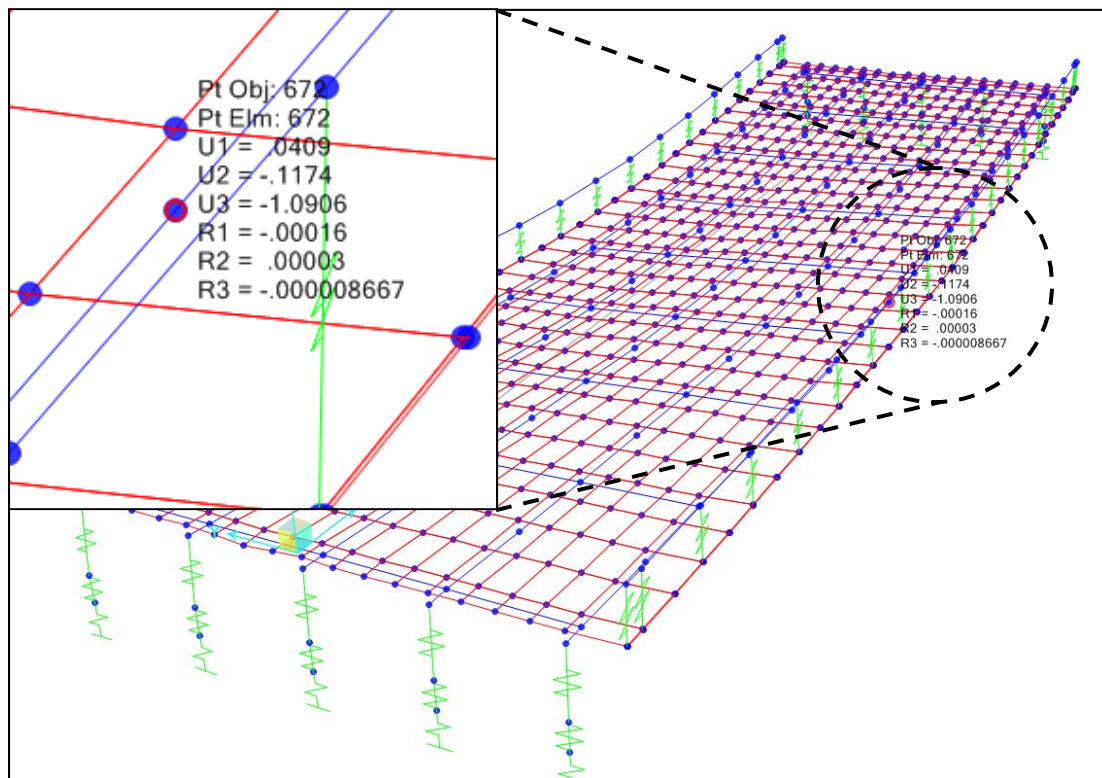


Figure 4.17: Deflection of LVDT1 node under test vehicle loading

## CHAPTER 5: PARAMETRIC STUDY

This chapter discusses the parametric study used to compare the effect of the AASHTO deflection limit on bridge vibration levels. Various designs are performed using high performance steel grades, and deck thickness is modified to bring the structure's vibration levels back down to a value similar to the original bridge design.

### 5.1 HPS Bridge Designs

Using the sample structure's span length, girder spacing, and overhang/barrier parapet arrangement, a series of designs were performed using the rapid steel girder design software MDX in accordance with the latest AASHTO specifications. The bridge was first redesigned using Grade HPS-50W steel with an eight inch thick composite concrete deck. This resulted in a much shallower section and a weight savings of over 20%. The design satisfied all AASHTO criteria including live load deflection. This section was then used as a basis for which to compare the rest of the parametric results, under the assumption that since the live load deflection criteria was satisfied, vibration effects would be controlled.

The bridge was then re-designed again to satisfy all AASHTO criteria, except the AASHTO recommended deflection limit of  $\frac{L}{800}$ , which allowed for a shallower section to be used. Designs utilizing a 9", 10", and 11" deck were then checked using the girder section produced from the eight inch deck design.

This process of designing the bridge for an eight inch deck slab and then checking for 9", 10" and 11" deck thicknesses was repeated for a hybrid steel girder section (HPS-70W flanges; HPS-50W web), and grade 100W steel section resulting in thirteen total designs. As anticipated, each increase in steel grade resulted in a shallower girder section. For each design, the maximum performance ratio (flexure controlled) was recorded in addition to the calculated deflection using the AASHTO recommended procedure of loading the structure with the maximum of a) the HS-20 design truck or b) 25% of the design truck plus lane loading. All girders were assumed to deflect equally and impact was included. Figure 5.1 and Table 5 present the girder section designs for various steel grades used in the parametric study and the corresponding maximum performance ratio (demand/capacity) and live load deflection. It should be noted that only the girders were designed in this study, diaphragms were not checked although their section properties were adjusted based on the web depth of the girders.

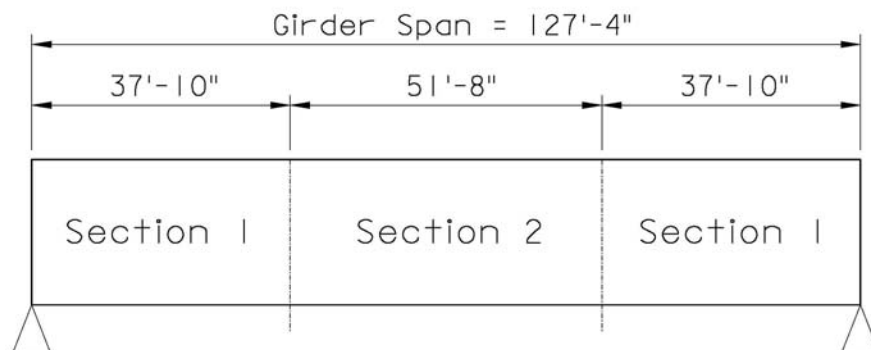


Figure 5.1: Girder design sections (see Table 5 for dimensions)

Design No.	Grade	Slab Thickness t <sub>s</sub> (in)	Web Depth D (in)	Web Thickness t <sub>w</sub> (in)	Girder Section 1				Girder Section 2				Max Perf. Ratio	AASHTO Deflection (in)
					T. Flange		B. Flange		T. Flange		B. Flange			
					b <sub>f</sub> (in)	t <sub>f</sub> (in)	b <sub>f</sub> (in)	t <sub>f</sub> (in)	b <sub>f</sub> (in)	t <sub>f</sub> (in)	b <sub>f</sub> (in)	t <sub>f</sub> (in)		
1	HPS-50W	8.00	50.00	0.50	18.00	0.75	22.00	1.00	18.00	0.875	22.00	1.25	0.953	1.818
2	HPS-50W	8.00	44.00	0.50	18.00	0.75	22.00	1.25	18.00	0.875	24.00	1.375	0.918	2.191*
3	HPS-50W	9.00	"	"	"	"	"	"	"	"	"	"	0.935	2.038*
4	HPS-50W	10.00	"	"	"	"	"	"	"	"	"	"	0.952	1.915*
5	HPS-50W	11.00	"	"	"	"	"	"	"	"	"	"	0.983	1.767
6	HPS-70W	8.00	40.00	0.50	18.00	0.625	22.00	1.00	18.00	0.75	22.00	1.125	0.936	3.050*
7	HPS-70W	9.00	"	"	"	"	"	"	"	"	"	"	0.945	2.819*
8	HPS-70W	10.00	"	"	"	"	"	"	"	"	"	"	0.973	2.610*
9	HPS-70W	11.00	"	"	"	"	"	"	"	"	"	"	0.998	2.421*
10	HPS-100W	8.00	35.00	0.50	16.00	0.75	18.00	1.13	16.00	0.75	18.00	1.25	0.941	4.003*
11	HPS-100W	9.00	"	"	"	"	"	"	"	"	"	"	0.951	3.670*
12	HPS-100W	10.00	"	"	"	"	"	"	"	"	"	"	0.963	3.371*
13	HPS-100W	11.00	"	"	"	"	"	"	"	"	"	"	0.977	3.104*

Table 5: HPS girder design results using MDX software (starred values indicate AASHTO deflection violation)



The design results in Table 4 are as expected. The flexural performance ratio increased with increasing slab thickness as the girder was required to support a larger dead load, thereby raising the demand while capacity remained constant. The maximum live load deflection decreased with increasing slab thickness as the composite section was made stronger. Figure 5.2 graphs the recorded live load deflection with relation to the slab thickness. The AASHTO  $\frac{L}{800}$  deflection limit is also shown, which for this structure was determined by:

$$\frac{(127' - 4'') \times 12}{800} = 1.91 \text{ inches}$$

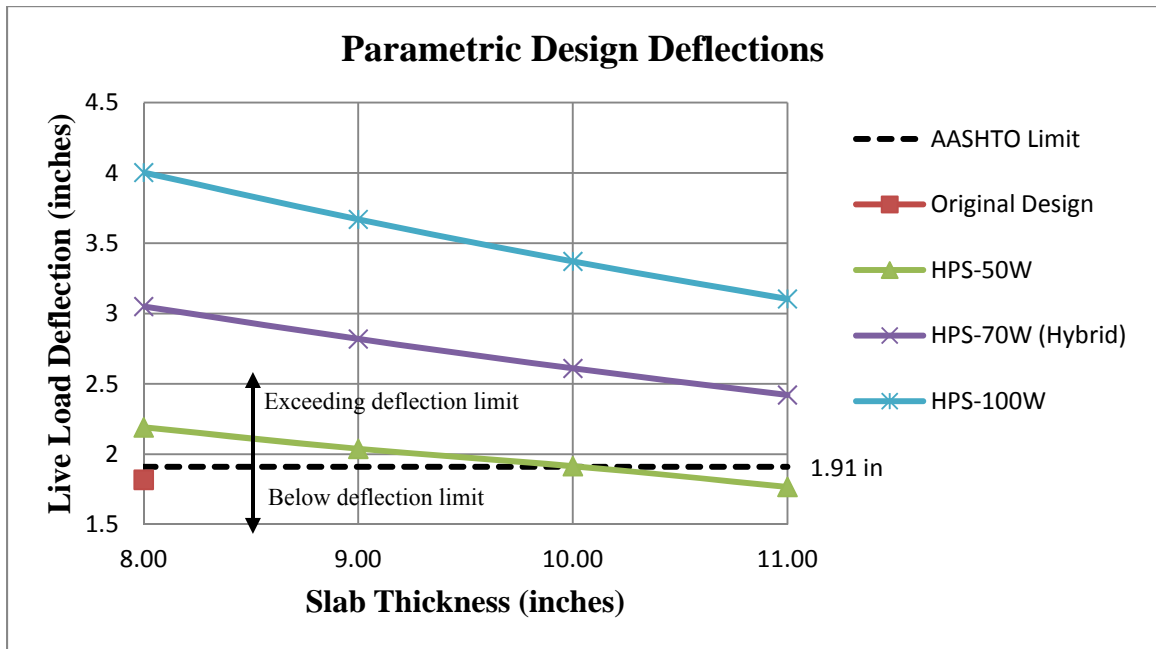


Figure 5.2: Graph of HPS design deflection vs. slab thickness

Note that design case 5 (HPS-50W with 11" slab) did not violate AASHTO deflection limits.

## 5.2 Dynamic Modeling

Following the completion of the design of a suite of different HPS bridges, each was modeled using the dynamic grillage program. Since the major geometry was not changed from the sample structure used for calibration, only the section properties of the elements needed to be changed. Transverse diaphragm element section properties were adjusted according to the web depth of the girder. The same truck and road roughness profile was used from the sample structure calibration model.

Each of the thirteen designs were tested under six separate loading conditions:

- 1) Truck in Lane 1 traveling 15 mph
- 2) Truck in Lane 1 traveling 35 mph
- 3) Truck in Lane 1 traveling 55 mph
- 4) Truck in Lane 2 traveling 15 mph
- 5) Truck in Lane 2 traveling 35 mph
- 6) Truck in Lane 2 traveling 55 mph

The maximum acceleration out of all six cases was then recorded and is presented in Table 6 below. The original HPS-50W design that satisfied the AASHTO deflection criteria produced a maximum acceleration of 23.31 in/sec<sup>2</sup>.

<b>Slab Thickness (in)</b>	<b>Maximum Acceleration (in/sec<sup>2</sup>)</b>		
	<b>HPS-50W</b>	<b>HPS-70W (Hybrid)</b>	<b>HPS-100W</b>
8.00	28.77	31.18	35.59
9.00	27.60	28.89	30.02
10.00	24.33	24.66	23.89
11.00	23.07	23.93	23.00

Table 6: Maximum acceleration for HPS bridges

The results follow closely to the anticipated behavior. A thicker deck section produced a decrease in the maximum acceleration. Additionally, a higher grade material (i.e. shallower section) produced an increase in the maximum acceleration. As shown in Figures 5.3, 5.4, and 5.5, the maximum amplitude can be seen for each of the design cases. Note that different truck speeds produced the maximum acceleration for separate design runs, which can be identified by the longer duration in the figures below.

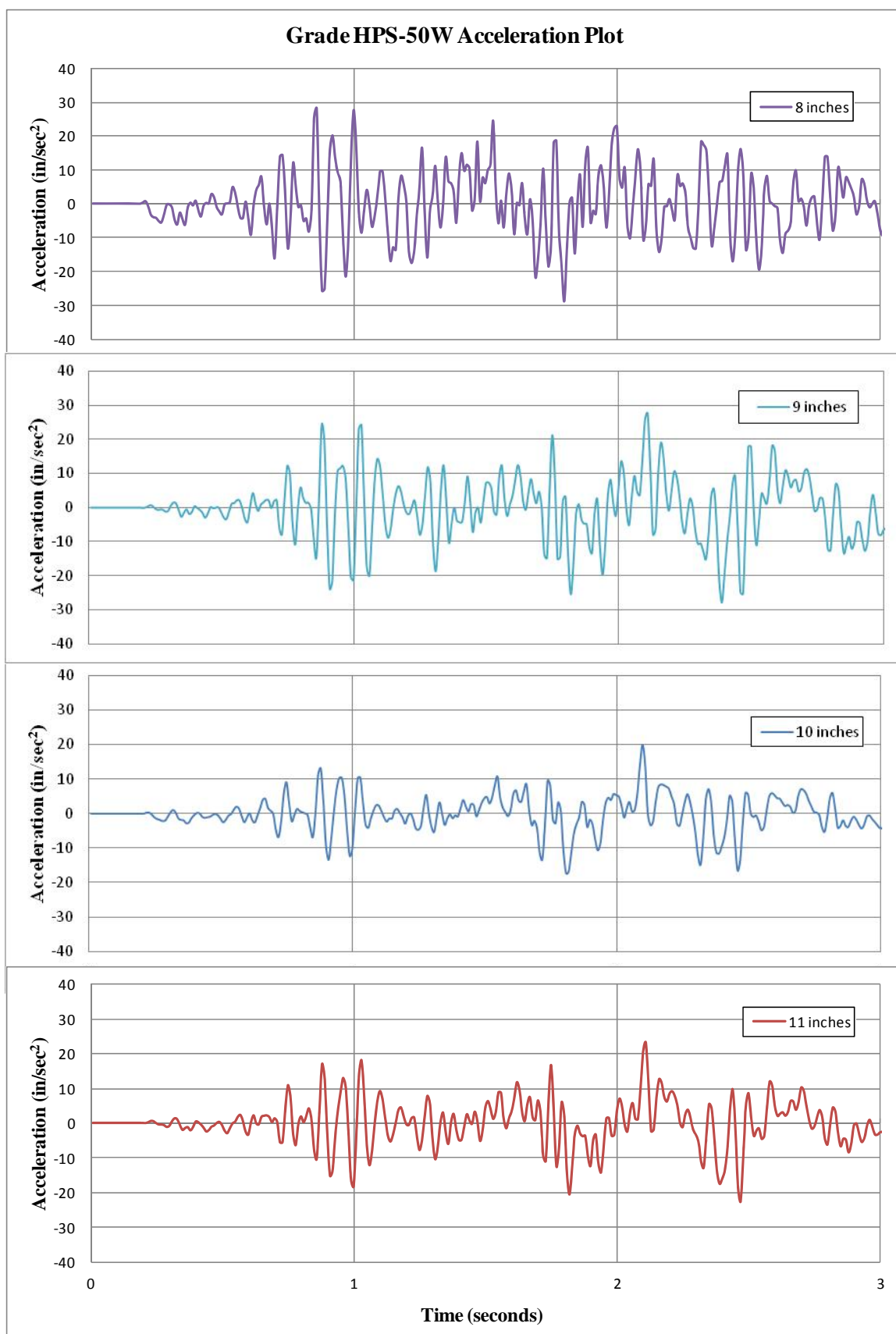


Figure 5.3: Grade HPS-50W acceleration plots

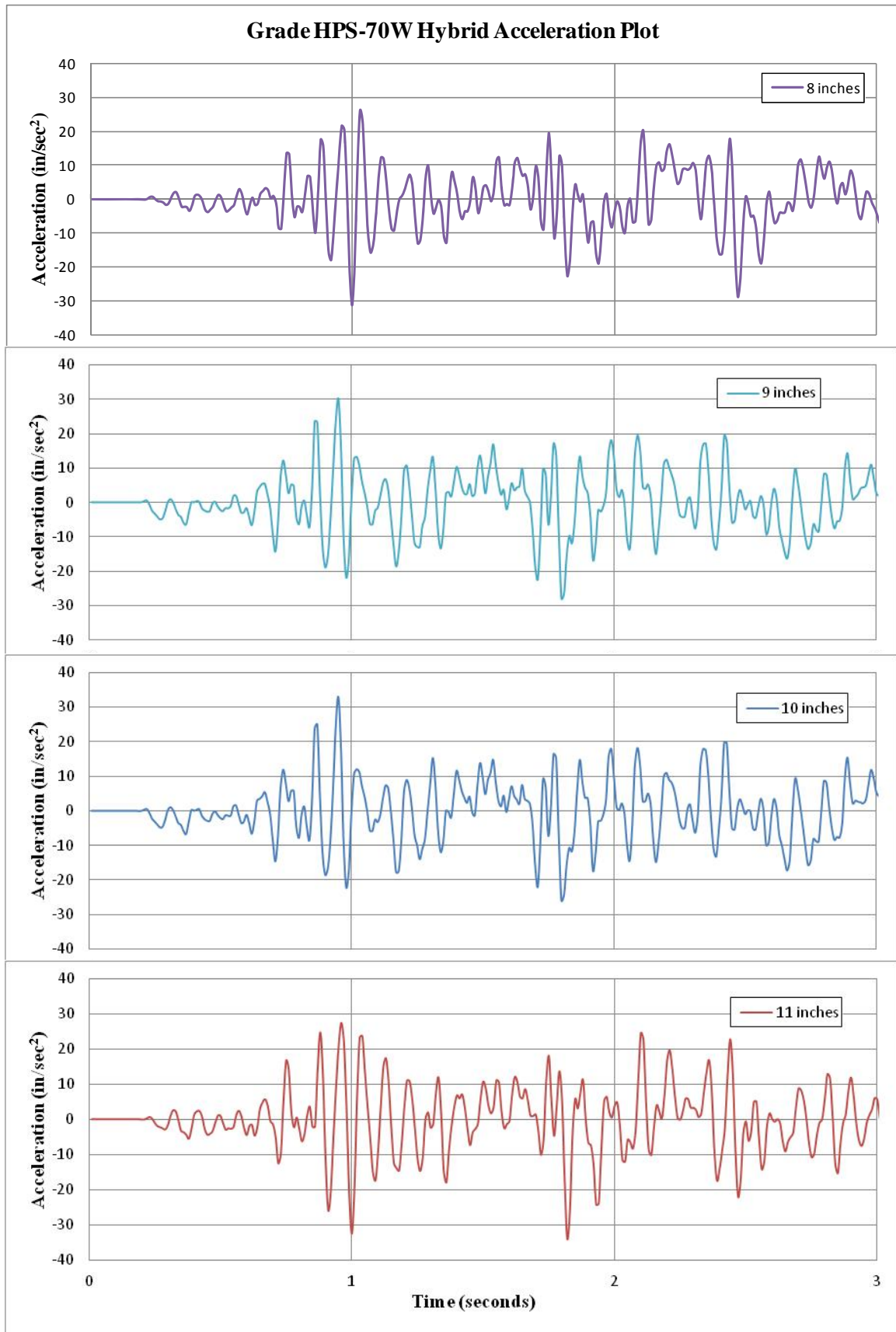


Figure 5.4: Grade HPS-70W Hybrid acceleration plots

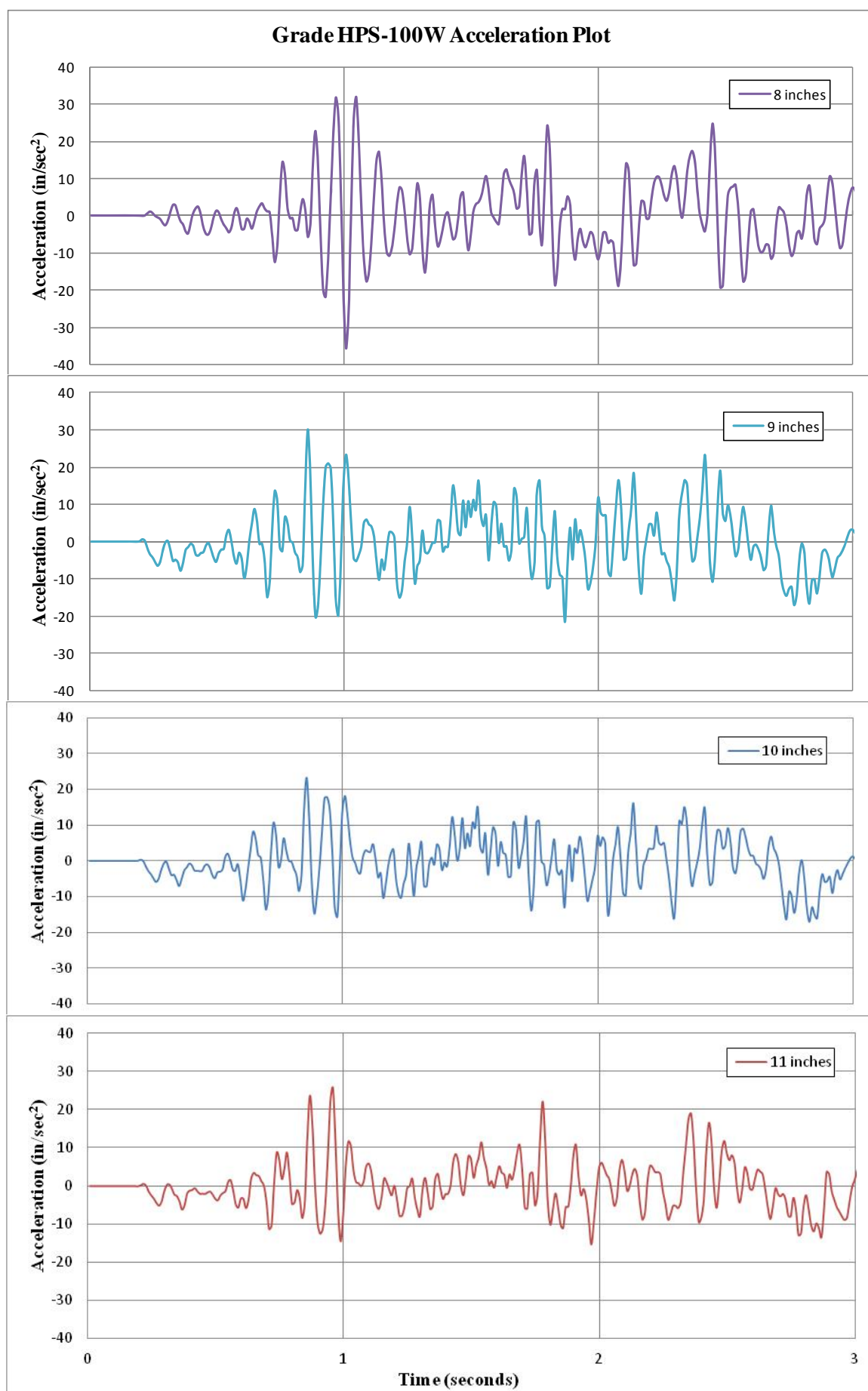


Figure 5.5: Grade HPS-100W acceleration plots

It is important to note that none of the parametric bridges exhibited accelerations over the “unpleasant” limit of  $50 \text{ in/sec}^2$  as derived by Wright and Walker. This could be due to the truck configuration and road roughness profile used in this study. These results should be viewed only within the context of the assumptions made. The maximum acceleration these bridges may see could vary greatly over time as the deck surface deteriorates and traffic loading becomes heavier.

However, the scope of this study is to emphasize the irrational role deflection limits play in HPS bridge design. The primary results of the parametric study can be shown in a graph of the maximum acceleration for each design case, which is presented in Figure 5.6 below.

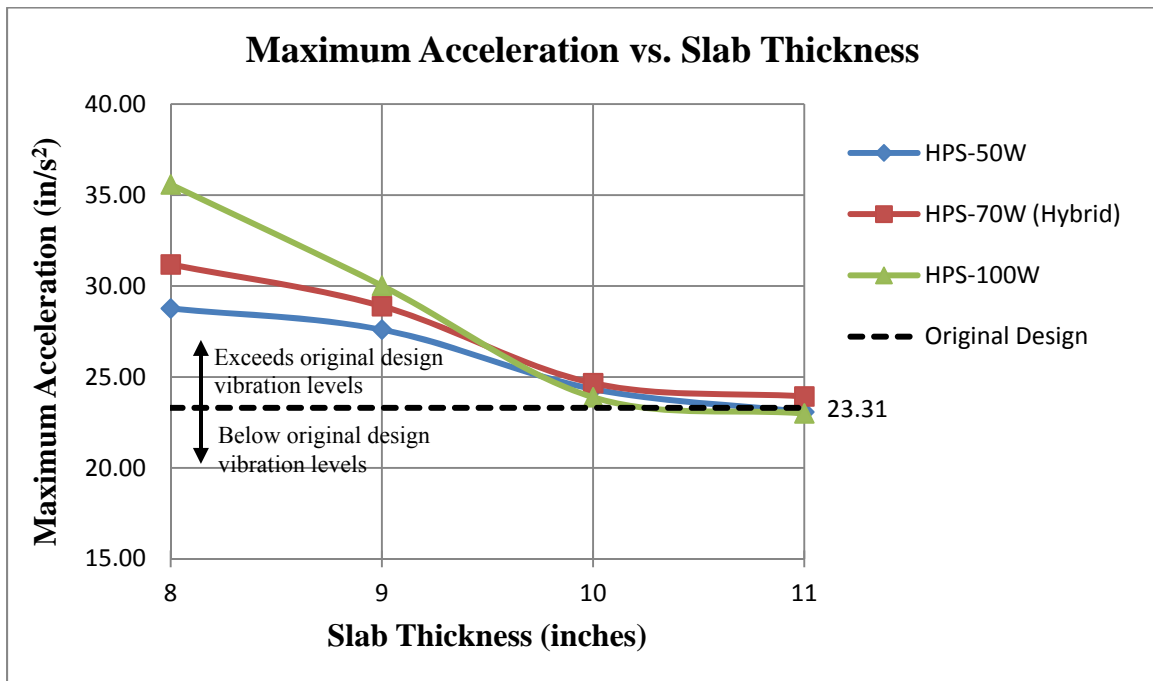


Figure 5.6: Maximum acceleration vs. slab thickness for various HPS bridge designs

Two important conclusions can be drawn from this figure:

- 1) While all designs violated the AASHTO deflection criteria (except case 5), none exceeded the unpleasant acceleration limit, indicating that the deflection limit does not correlate with maximum vibration. Despite the reported values not necessarily representing the lifetime maximum acceleration these bridges may see, the trend still disassociates the deflection limit with vibration control.
- 2) All designs with an eight-inch thick slab had higher acceleration values than the original HPS-50W design (which met AASHTO deflection criteria). However, by increasing the slab thickness for each girder section, the maximum acceleration value converged back to the down to the original level. This suggests that despite failing to meet the deflection limit, all designs were able to achieve the same level of vibration as the first structure.



## CHAPTER 6. CONCLUSIONS AND RECOMMENDATIONS

This thesis used a dynamic bridge-road-vehicle grillage analysis program to compare the interaction of live load deflection limits and vibration levels. A sample structure was first modeled and calibrated using field measured data. Working from the initial model, a parametric study was performed on a series of AASHTO-designed High Performance Steel girder bridges. Structures using steel girders of grades 50, 70, and 100 ksi with deck thicknesses ranging from 8" to 11" were designed in accordance with all code provisions barring the recommended deflection criteria. The grillage program was then used to determine the maximum acceleration experienced by each design.

The results showed that the AASHTO recommended deflection limit of  $\frac{L}{800}$  provided no control on the structures' vibration levels. All designs, while violating the deflection criteria, displayed maximum acceleration values well under what a typical human response would consider uncomfortable.

Additionally, a design was performed for a Grade 50 structure that complied with the AASHTO deflection limit. The maximum acceleration this structure exhibited was able to be achieved by each of the designs in violation of the deflection limit. Increasing the deck thickness on designs which used a shallower section significantly reduced the amount of vibration experienced.

## REFERENCES

AASHTO LRFD Bridge Design Specifications, Customary U.S. Units, 6<sup>th</sup> Edition, 2012

ASCE. "Deflection Limitations of Bridges." Progress Report of the Committee on Deflection Limitations of Bridges of the Structural Division. Journal of the Structural Division. Vol. 84, no. 3, 1958.

Azizinamini, A., Barth, K., Dexter, R., Rubeiz, C., "High Performance Steel: Research Front- Historical Account of Research Activities." Journal of Bridge Engineering. v 9, n 3, pp. 212-217, 2004

Boothby, T. E. and Laman, J. A., "Cumulative Damage to Bridge Concrete Deck Slabs Due to Vehicle Loading." Journal of Bridge Engineering. v 4, n 1, 1999.

Burke, M. P., "Superstructure Flexibility and Disintegration of Reinforced Concrete Deck Slabs: An LRFD Perspective." Transportation Research Record No. 1770, pp. 76-83, 2001.

CSi Bridge Software<sup>®</sup>, Rapid Bridge Design and Analysis. © 2013 Computer and Structures, Inc.

Demitz, J.R., Mertz, D.R., Gillespie, J.W., "Deflection Requirements for Bridges Constructed With Advanced Composite Materials." Journal of Bridge Engineering. v 8, n 2, pp. 73-83, 2003.

Fanning, P.J., "Pedestrian Bridge Vibration Serviceability: A Case Study in Testing and Simulation." Advances in Structural Engineering. v 13, n 5, pp. 861-873, 2010.

Felkel, J.P., Rizos, D.C., Ziehl, P.H., "Structural Performance and Design Evaluation of HPS 70W Bridge Girders." Journal of Constructional Steel Research. v 63, n 1, pp. 909-921, 2007.

Fountain, R.S., Thunman, C.E., "Deflection Criteria for Steel Highway Bridges." Presented at National Engineering Conference, New Orleans, LA, April, 1987.

Gindy, M. "Development of a Reliability-Based Deflection Limit State for Steel Girder Bridges." PhD Dissertation. Rutgers, State University of New Jersey, Piscataway, 2003.

Goodpasture, D. W. and Goodwin, W. A. "Final Report on the Evaluation of Bridge Vibration as Related to Bridge Deck Performance." The University of Tennessee and Tennessee Department of Transportation, 1971.

Kulicki, J., "Implementation of HPS in Bridge Design." Restructuring America and Beyond: Proceedings of Structure Congress XII, April 2-5, v 1, pp. 157-172, 1995.

Liu, M., "A Three-Dimensional Dynamic Model For Bridge-Road-Vehicle System." MS Dissertation, Department of Civil and Environmental Engineering, Bradley University, 1996.

Macioce, T., "HPS Demonstration Project: The Ford City Bridge." Proceedings of the 1999 Structures Congress, April 18-21, v 1, pp. 753-756, 1999.

Mastaglio, L., "HPS Moves Ahead for Bridge Design." Better Roads, v 73, n 5, pp. 70-73, 2003.

MDX Software<sup>®</sup>, Curved & Straight Steel Bridge Design & Rating for Windows. © 2013 MDX Software, Inc.

Nassif, H., Liu, M., Su, D., Gindy, M., "Vibration Versus Deflection Control for High-Performance Steel (HPS) Girder Bridges." Transportation Research Board. v 2251, pp. 24-33, 2011.

Oehler, L.T., "Vibration Susceptibilities of Various Highway Bridge Types." Michigan State Highway Department. Project 55 F-40 No. 272, 1957.

Oehler, L.T., "Bridge Vibration- Summary of Questionnaire to State Highway Departments." Highway Research Circular. n 107, 1970.

Roeder, C.W., Barth, K.B., Bergman, A., "Improved Live Load Deflection Criteria for Steel Bridges." Final Report NCHRP 20-07/133, University of Washington, Seattle, WA, 2002.

Sause, R., "Cost Effective Bridge Design Using High Performance Steel (HPS)." International Symposium on Steel for Fabricated Structures, v 1, pp. 3-10, 1999.

Wilson, A.D., Gross, J.H., Stout, R.D., Asfahani, R.L., Manganello, S J., "Development of an Improved HPS-100W Steel for Bridge Applications." Proceedings from the Materials Solutions Conference, v 1, pp. 32-42, 2002.

Wright, R.N., Walker, W.H., "Criteria for Deflection of Steel Bridges." Bulletin for the American Iron and Steel Institute. n 19, 1971.

Wu, H., "Influence of Live-Load Deflections on Superstructure Performance of Slab on Steel Stringer Bridges." Ph.D. Dissertation, Department of Civil and Environmental Engineering, West Virginia University, 2003.

Yakel, A., "Flexural Capacity and Ductility of HPS-70W Bridge Girders." Engineering Journal, v 39, n 1, pp. 38-51, 2002.